Diphenylamine-substituted osmanaphthalyne complexes: structural, bonding, and redox properties of unusual donor–bridge–acceptor systems

Article

Accepted Version

Diphenylamine-Substituted Osmanaphthalyne Complexes: Structural, Bonding and Redox Properties of Unusual Donor−Bridge−Acceptor Systems

Ming-Xing Zhang,[a] Jing Zhang,[a] Xuyang Jin,[a] Xiaona Sun,[a] Jun Yin,[a] František Hartl,*[,b] Sheng Hua Liu*[,a]

[a]*Key Laboratory of Pesticide and Chemical Biology, Ministry of Education, College of Chemistry, Central China Normal University, Wuhan 430079, P.R. China*

[b]*Department of Chemistry, University of Reading, Whiteknights, Reading RG6 6AD, UK*

Abstract

Diarylamine-substituted osmanaphthalyne complexes featuring two redox centers linked by the rigid skeleton of the metallacycle (C ^ C^+), viz. [$OsCl_2(PPh_3)_2${(C ^ C^+)NAr_2}][BF_4^-] (Ar = Ph (**1a**), *p*-MeOPh (**1b**)) and their open-ring precursors [$OsHCl_2(PPh_3)_2${(≡C–C(PPh_3^+)=CHPh)NR_2}][BF_4^-] (Ar = Ph (**2a**), *p*-MeOPh (**2b**)), were successfully synthesized and characterized by ^{1}H, ^{13}C and ^{31}P NMR spectroscopy, ESI-MS, and elemental analysis. The solid-state molecular structures of complexes **1a** and **2a** were ascertained by single-crystal X-ray diffraction. The Os≡C bond length in both **1a** and **2a** falls within the range reported for similar osmanaphthalynes and osmium carbyne complexes, respectively. The structural parameters determined for **1a**, appreciably reproduced by theoretical calculations, point to a π-delocalized metallacycle structure. The purple colour of **1a** and **1b** is determined by diarylamine→Os(metallacycle) charge transfer absorption in the visible region. The neutral, one-electron-oxidized and one-electron reduced states of **1a**, **1b** and a reference complex lacking the diarylamine substituent, [$OsCl_2(PPh_3)_2${(C^C^+)}][BF_4^-] (**1′**), were investigated by cyclic and square-wave voltammetry, UV-vis-NIR spectroelectrochemistry, and DFT calculations. The spin density

in singly oxidized [**1a**]$^{+}$ and [**1b**]$^{+}$ is dominantly residing on the aminyl segment, with osmium involvement controlled by the diphenylamine substitution. Spin density in stable singly-reduced [**1'**]$^{-}$ is distributed mainly over the osmanaphthalyne metallacycle.

Keywords: Osmanaphthalyne metallacycle; Diphenylamine donor; Redox states; DFT calculations; Spectroelectrochemistry.

Introduction

Three years after Thorn and Hoffmann had predicted the existence of transition metal heteroaromatics,[1] Roper and co-workers reported in 1982 the first isolated metallabenzene.[2] Since then, the chemistry of transition metal-containing aromatics has attracted considerable attention, both experimentally and theoretically, and an impressive progress has been made in this field of organometallic chemistry. Several types of third-row late-transition-metal heteroaromatics, including metallabenzene,[2,3] metallafuran,[4] metallabenzyne,[5] metallapyridine,[6] metallanaphthalene,[7] metallanaphthalyne,[8] metallapentalynes, metallapentalenes and their derivatives[9] were successfully isolated and characterized in the past decades. A unique cyclic second-row transition metal-carbyne complex (ruthenapentalyne with a strongly bent Ru≡C–C moiety) has recently been reported by Xia and co-workers.[10] Displaying both aromaticity of fused organic heterocyclic compounds and characteristics of organometallics, these compounds have attracted wide attention of an increasing numbers of researchers. Over the past few years, the studies mainly focused on their reactivity.[11] However, other special features such as optical[12] and magnetic[13] have gradually been discovered and reported. At the same time, studies of redox properties of such metallacycles (e.g., osmabenzene[14]) are scarce.

Mixed-valence (MV) compounds have been investigated intensively over the past half century.[15] According to Creutz and Taube, the most common MV compounds are represented by the general formula [M_a^n–BL–M_b^{n+1}], where BL refers to an organic bridge

and M_a and M_b are usually redox-active inorganic or organometallic redox centers.[16] Transition metal complexes decorated with additional redox-active units represent one type of promising photoelectric materials that display intriguing electrochemical and photophysical properties and are potentially useful for applications in molecular electronics,[17] information storage,[18] charge-transporting,[19] light scavenging and solar cells.[20] In most cases, the BL backbones in these MV systems are readily oxidizable organic bridge cores, for example, unsaturated sp/sp^2-carbon-based chains (oligoyne, oligoene) or fused aromatic rings (heterocycles, oligoacene).[21] However, a mixed-valence system bridged by the backbone of a metallacycle has remained largely unexplored.[22] Pertinent information obtained from studies of charge-transfer processes in such systems is supposed to pave a way to design and syntheses of new kinds of organometallic molecular wires.

Triarylamines, NAr_3, are most widely studied among diverse redox-active groups in organic MV systems, both in the bridging and terminal positions.[23] The readily accessible $NAr_3/NAr_3^{\bullet+}$ redox process and good stability of the oxidized $NAr_3^{\bullet+}$ species are highly advantageous.[24] Moreover, their good electron-donating and hole-transporting abilities make them widely used in optoelectronic devices.[25] Based on our recent studies of aminophenylferrocene and diphenylaminoferrocene,[26] (methoxy-substituted) diphenylamine (NAr_2) as a terminal group lowers the anodic potential of the Fe(II) centre due to its donor capacity while not integrating itself with the adjacent ferrocenyl Cp ring into a single redox-active unit but showing an independent irreversible anodic wave. More integration is expected when binding NAr_2 to an aromatic ring system of a metallacycle.

Herein, we report a new kind of asymmetric donor-bridge-acceptor (D−B−A) system, where D stands for redox active diphenylamine, A for the metallacycle acceptor of osmanaphthalyne and B for the osmanaphthalyne backbone. The synthetic routes toward the metallacycle in the studied osmanaphthalyne complexes **1a** and **1b** have been based on C–H activation reactions (see Scheme 1). The thorough study of their structural, spectroscopic, and redox properties provides detailed understanding of the charge-transfer

characteristics in these hybrid D−B−A systems, being complemented by quantum chemical calculations to rationalize the electrochemical and spectroscopic observations. To the best of our knowledge, this is the first spectro-electrochemical study of the redox behavior of a metallanaphthalyne system reported to date.

Results and Discussion

Syntheses and Characterization

Unsubstituted reference compound **1′** was synthesized following a reported procedure.[27] An alternative photochemical route to **1′** has recently been published by our group.[28] The general synthetic route to osmanaphthalyne complexes **1a** and **1b** is outlined in Scheme 1. Intermediates **3a** and **3b** were obtained in high yields by nucleophilic addition of HC≡CMgBr to corresponding aldehydes. The target cationic osmanaphthalyne compounds were then obtained by intramolecular C−H activation of precursor alkenyl carbynes **2a** and **2b** under an O_2 atmosphere in moderate yields. The addition of the diphenylamino substituets to **1′** does not compromise the stability of the osmanaphthalyne system protected by the bulky phosphonium substituent, under ambient conditions. Notably, the original green color of **1′** turns deep purple for **1a** and **1b**, due to a new low-lying charge-transfer electronic transition discussed in detail hereinafter in the theoretical section. All the three osmanaphthalyne complexes are readily soluble in common organic solvents of different polarity, such as dichloromethane, chloroform, acetone, acetonitrile, or tetrahydrofuran (THF). Remarkably, though, no solvatochromism was observed for **1a**.

NMR spectra exhibit important features proving the existence of the osmium carbyne unit in the open and ring structures. The ^{1}H NMR signal of the hydride ligand at Os was found at ca. -6.2 ppm for both **2a** and **2b**, and the characteristic low-field signal of ≡C–C(PPh_3^+)=C*H* was also observed at 9.69 and 9.66 ppm, respectively. In the ^{13}C NMR spectra of **2a** and **2b**, the signals at 252.6 and 253.6 ppm, respectively, have been attributed to Os≡*C*. For **1a** and **1b**, the ^{13}C NMR resonance of Os≡*C* shifts to 267.9 and 269.2 ppm,

respectively, which is close to the value of 264.9 ppm reported[27] for osmanaphthalyne **1′**.

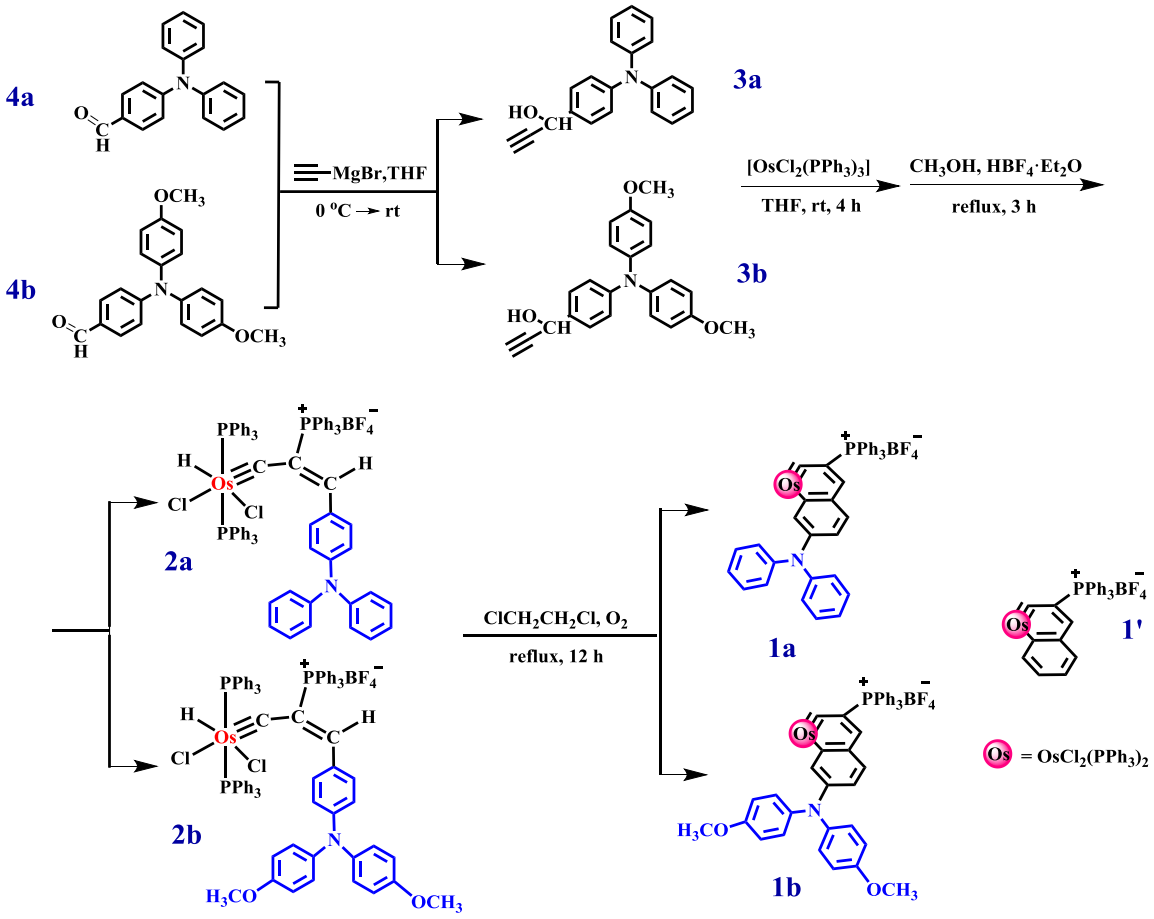

Scheme 1. General synthetic routes toward complexes **1a** and **1b,** and the molecular structure of reference[27] complex **1′**.

X-ray Crystallography

Complexes **1a** and **2a** have been structurally characterized by single-crystal X-ray diffraction (Figures 1 and 2, Table 1, and ESI, Tables S1-S4). For complexes **1a** and **2a**, crystals suitable for the X-ray analysis were grown at room temperature from a dichloromethane solution layered with hexane (**1a**) and tetrahydrofuran (**2a**). Complex **2a** crystallized with two and a half dichloromethane molecules in the unit cell (ESI, Table S1). The crystal structure of **2a** (Figure 1) shows the short Os1–C1 bond of 1.701(10) Å falling within the range of Os≡C bond lengths reported for osmium carbyne complexes (1.694(4)–

1.841(16) Å).[29] The C1–C2 and C2–C21 distances of 1.461(13) Å and 1.399(14) Å, respectively, lie between the values characteristic of C–C and C=C bonds. The C2–C1–Os1 (174.2(7)º) bond angle reaches nearly the ideal value of 180º, slightly exceeding those reported for $[OsH(\kappa^2\text{-}O_2CCH_3)(\equiv CCH{=}CPh_2)(P\textit{i}Pr_3)_2]BF_4$ (171.2(3)º)[30] and $[OsH(\equiv CCH{=}CPh_2)(H_2O)_2(P\textit{i}Pr_3)_2][BF_4]_2$ (168.0(5)º).[31] It is worth noting that, compared to a very close osmium carbyne complex (with terminal phenyl instead of TPA),[13] the Os≡C bond in **2a** is shorter and the C2–C1–Os1 bond angle closer to 180º (ESI, Table S5). In the DFT-optimized molecular geometry of **2a** (ESI, Figure S1), the N–C bond linking the diphenyl amine (DPA) substituent to the vinyl benzene ring (1.377 Å) is much shorter compared to the two N–C(phenyl) bonds (1.438 Å and 1.439 Å), in agreement with the crystal data for **2a** (Table S4). This difference may reflect some electronic interaction between the osmium center and the diphenylamine substituent. The C1–C2–C21 and C2–C21–C22 bond angles are 125.9(8) and 131.8(10)º, respectively. In line with structural data reported for a similar phenyl-terminated osmium carbyne complex,[13] the existence of the alkenyl carbyne backbone in **2a** (Scheme 1) is obvious.

Target complex **1a** contains an essentially planar osmanaphthalyne unit (Figure 2). The sum of angles in the ring constructed by Os1, C21, C20, C19, C16, and C17 is 718.8°, which is very close to the value of 720° for the ideal aromatic benzene ring. For comparison, unsubstituted complex **1′** exhibits the value of 719.9°.[27] It is worth mentioning that the Os1−C21 (1.740(5) Å) and Os1−C17 (2.117(5) Å) bond lengths fall within the range typical for Os≡C bonds (1.694(4)–1.841(16) Å)[29,32] and Os−C(aryl) bonds (2.02–2.18Å),[33] respectively. They are also very close to the corresponding values determined for the osmanaphthalyne reported by Jia and co-workes, viz. 1.732(4) Å and 2.127(3) Å, respectively.[34] The other bonds in the metallacycle lie within the C–C and C=C bond length interval, without significant alternation, suggesting a delocalized ring structure. The Os1–C21–C20 bond angle reaches 152.8(4)°, which is similar to values encountered in Jia's osmanaphthalyne (155.0(3)°) and osmabenzynes (148.3(6)–154.9(9)°).[5c,29] The crystal

data have been well reproduced in the corresponding DFT (G09-B3LYP)-optimized structure presented in Table 1 and Table S2.

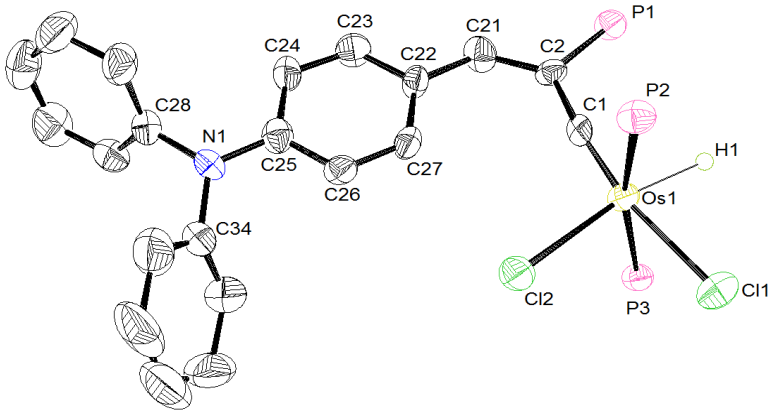

Figure 1. X−ray crystal structure of **2a** (terminal TPA) shown with thermal ellipsoids at the 50% probability level. The phenyl moieties in PPh_3 (P2, P3) and PPh_3^+ (P1), the counter anion (BF_4^-), hydrogen atoms (except the hydride ligand at Os, H1) and the co-crystallized dichloromethane molecules are omitted for clarity.

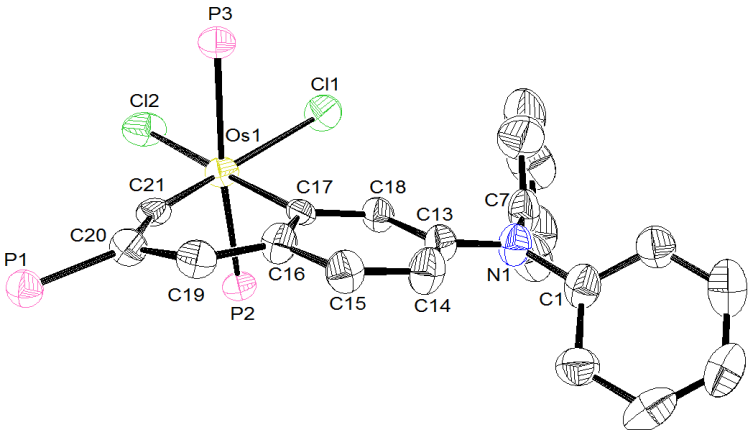

Figure 2. X−ray crystal structure of **1a** shown with thermal ellipsoids at the 50% probability level. The phenyl moieties in PPh_3 (P2, P3) and PPh_3^+ (P1), the counter anion (BF_4^-), and hydrogen atoms are omitted for clarity.

Table 1. Selected bond lengths (Å) and angles (deg) for complex **1a** and its DFT (G09-B3LYP)-optimized structure.

Parameter	Crystal	Calculated
Os(1)−C(21)	1.740(5)	1.760
Os(1)−C(17)	2.117(5)	2.136
C(13)−N(1)	1.380(7)	1.379
C(13)−C(14)	1.406(8)	1.429
C(13)−C(18)	1.410(8)	1.415
C(14)−C(15)	1.358(8)	1.363
C(15)−C(16)	1.423(8)	1.437
C(16)−C(19)	1.396(7)	1.405
C(16)−C(17)	1.447(7)	1.466
C(17)−C(18)	1.369(7)	1.393
C(19)−C(20)	1.416(8)	1.415
C(20)−C(21)	1.388(7)	1.387
C(21)−Os(1)−C(17)	81.0(2)	82.5
N(1)−C(13)−C(14)	121.4(5)	119.8
N(1)−C(13)−C(18)	119.4(5)	121.1
C(14)−C(13)−C(18)	119.2(5)	119.0
C(15)−C(14)−C(13)	118.8(5)	118.8
C(14)−C(15)−C(16)	122.6(5)	122.7
C(19)−C(16)−C(15)	115.6(5)	114.9
C(19)−C(16)−C(17)	125.4(5)	125.5
C(15)−C(16)−C(17)	118.8(5)	119.5
C(18)−C(17)−C(16)	116.6(5)	115.4

C(18)−C(17)−Os(1)	119.4(4)	122.2
C(16)−C(17)−Os(1)	123.9(4),	122.3
C(17)−C(18)−C(13)	123.7(5),	124.4
C(16)−C(19)−C(20)	124.0(5)	125.6
C(21)−C(20)−C(19)	111.6(5)	111.4
C(20)−C(21)−Os(1)	152.8(4)	152.0

Electrochemical Studies

The redox properties of cationic osmanaphthalyne complexes **1′**, **1a** and **1b** were studied by cyclic voltammetry (CV) and square-wave voltammetry (SWV) in deaerated dry dichloromethane containing 0.1 M *n*-Bu_4NPF_6 as the supporting electrolyte (Figure 3). The relevant electrochemical data are presented in Table 2.

As shown in Figure 3, reference complex **1′** exhibits two reversible redox processes, viz. reduction to $[\mathbf{1'}]^-$ at $E_{1/2} = -1.19$ V, and oxidation to $[\mathbf{1'}]^+$ at $E_{1/2} = +1.20$ V vs. Fc/Fc^+. Compound **1a** containing the diphenylamine substituent exhibits three redox steps within the available potential window. The cathodic wave at $E_{1/2} = -1.42$ V assigned to the reduction of [**1a**] to $[\mathbf{1a}]^-$, is shifted negatively from reference **1′**, reflecting the amine donor power. In the anodic region, the first reversible oxidation at $E_{1/2} = +0.88$ could be attributed either to the oxidation of the diphenylamine group or the osmanaphthalyne metallacycle. Combination of cyclic voltammetry with UV-vis spectroelectrochemistry and theoretical calculations in the following sections prioritizes the diphenylamine oxidation. The subsequent metallacycle-localized irreversible oxidation of $[\mathbf{1a}]^+$ at $E_{p,a} = +1.68$ V is shifted positively compared to that of **1′** due to the electron-deficient aminium substituent on the metallacycle. Both anodic waves of **1b** bearing the stronger bis(4-methoxyphenyl)amine donor, are negatively shifted compared to **1a**; the second oxidation generating $[\mathbf{1b}]^{2+}$ becomes more reversible due to the stabilizing effect of the methoxy

groups. On the other hand, both [**1a**]$^{-}$ and [**1b**]$^{-}$ are less stable than [**1′**]$^{-}$ lacking the amine substituents. This is documented by the irreversible reduction of **1a** and **1b** ($I_{p,a}/I_{p,c} < 1$). The reverse anodic scan triggered beyond the parent cathodic waves shows in both cases a new anodic wave beyond the parent anodic counterwave due to a secondary oxidized species. The cathodic spectroelectrochemistry at ambient conditions in the following section was therefore carried out only for **1′**.

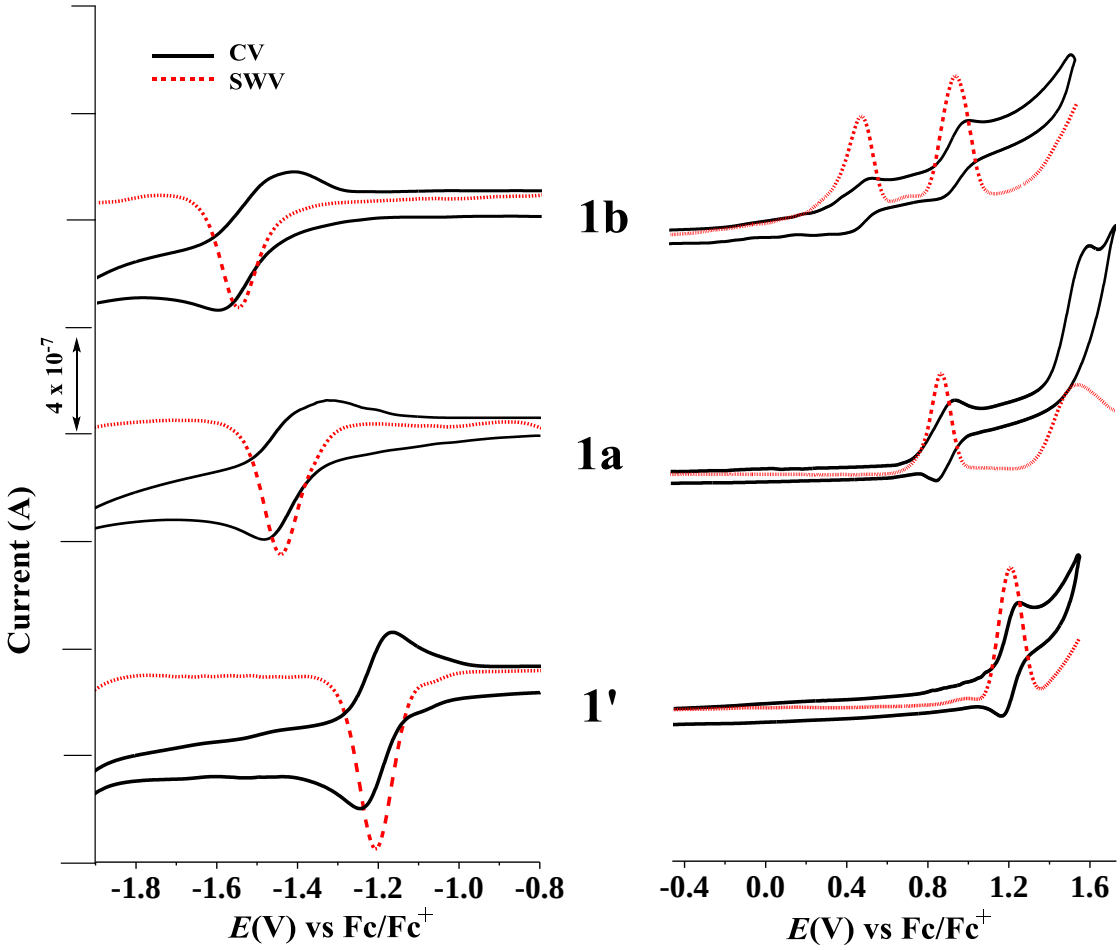

Figure 3. Left: cyclic voltammograms (CV) of complexes **1′**, **1a**, **1b** in CH_2Cl_2/*n*-Bu_4NPF_6 at v = 50 mV s^{-1}. Right: corresponding square-wave voltammograms (SWV) of complexes **1′**, **1a**, **1b** at f = 10 Hz and t_p = 25 mV.

Table 2. Electrochemical data[a,b] for complexes **1′**, **1a** and **1b**.

Complex	$E_{1/2}(1)$ / V (ΔE_p / mV)	$E_{1/2}(2)$ / V (ΔE_p / mV)	$E_{1/2}(3)$ / V (ΔE_p / mV)
1′	–1.19 (72)	--	+1.20 (70)
1a	–1.39 (100)	+0.89 (90)	+1.60 [c]
	–1.34 [d]	+0.81	+1.34
1b	–1.52 (135)	+0.48 (80)	+0.94 (100)

[a] All the redox potentials are referenced against the standard ferrocene/ferrocenium (Fc/Fc^+) couple at (v = 0.05 V s^{-1}). [b] Potential values determined in dichloromethane/10^{-1} M *n*-Bu_4NPF_6, unless stated otherwise. [c] $E_{p,a}$ value. [d] Acetonitrile /10^{-1} M *n*-Bu_4NPF_6. (Under the experimental conditions used in this work, $E_{1/2}$ (Fc/Fc^+) = +0.46 V vs Ag/Ag^+ in dichloromethane and +0.43 V vs Ag/Ag^+ in acetonitrile; ΔE_p (Fc/Fc^+) = 70 mV in dichloromethane.)

UV-visible Electronic Absorption of Parent Osmanaphthalynes

Electronic absorption spectra of osmanaphthalynes **1′**, **1a** and **1b** in the UV-vis region are shown in Figure 4. All three complexes feature a distinct absorption band between 15000-25000 cm^{-1} (Table 3), which determines their color. The lowest-energy absorption of purple **1a** and **1b** is significantly red-shifted compared to that of green reference **1′**. This section will focus on the analysis of this dominant absorption feature to understand the difference in the electronic properties between the amine-appended and unsubstituted osmanaphtalynes.

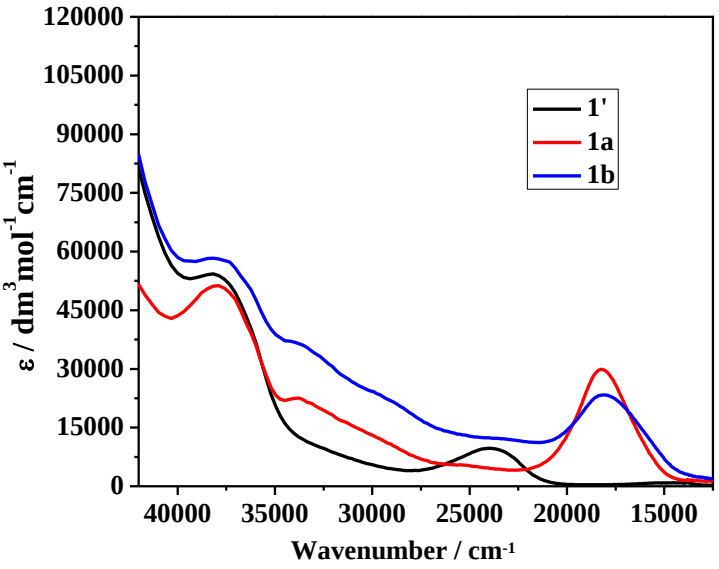

Figure 4. UV-vis electronic absorption spectra of **1a**, **1b** and reference complex **1′** (10^{-5} M) in CH_2Cl_2 at 298 K.

Quantum mechanical calculations, presented in detail hereinafter, have revealed that the lowest-energy electronic excitation of diphenylamine (DPA)-substituted **1a** has a dominant (95%) HOMO→LUMO character and can be assigned to the DPA→Os(metallacycle) charge transfer, resulting in a charge separated excited state. The experimental lowest-energy absorption maximum at 18300 cm^{-1} (calculated at 19300 cm^{-1}, Table 4), roughly corresponds (within 1500 cm^{-1}) with the HOMO-LUMO gap estimated from the CV data of **1a** (Table 2), thereby providing strong support for the TDDFT assignment. For closely related **1b**, the lowest absorption maximum at 18100 cm^{-1} (calculated at 17750 cm^{-1}) deviates appreciably from the estimated HOMO-LUMO gap, by additional 2000 cm^{-1} compared to **1a**. The difference can be explained by the reduced (64%, Table 4) HOMO→LUMO contribution in this case. Much larger deviation applies to **1′** absorbing at 24100 cm^{-1} (calculated at 24500 cm^{-1}) where the difference from the estimated HOMO-LUMO gap increases by additional 3000 cm^{-1} compared to **1b**. The significant blue shift of the lowest electronic absorption compared to **1a**, and the big difference from

the estimated HOMO-LUMO gap reflect a different nature of the electronic excitation involving a lower-lying occupied orbital, viz. HOMO-7→LUMO (79%, Table 4), which originates in the absence of DPA from the Os-bound Cl^- and PPh_3 donor ligands, Cl^-/PPh_3→Os(metallacycle).

It is worth mentioning that despite the strong charge-transfer character of the lowest electronic excitation in **1a**, the corresponding absorption band does not show any apparent solvatochromism, as documented by the results collected in ESI, Table S6 and corresponding Figure S3. A plausible explanation for this behaviour is the same absolute molecular dipole, but with changed polarity signs, in the ground state and the lowest optically populated excited state of **1a**.[35]

Table 3. UV−Vis−NIR electronic absorption of complexes **1′**, **1a**, **1b** and their different redox forms in dichloromethane/*n*-Bu_4NPF_6.

Complex	$\tilde{\upsilon}_{max}$ (cm^{-1}) (ε_{max} ($dm^3\ mol^{-1}\ cm^{-1}$))
1′	23950 (10100), 38100 (54350)
[1′]$^+$	ca. 19600 [a]
[1′]$^-$	24100 (6550)
1a	18300 (30100), 38050 (51300)
[1a]$^+$	11400 (4900), 14450 (13550)
1b	18100 (23500), 38050 (58350)
[1b]$^+$	12550 (5600)

[a] Poorly resolved weak and broad absorption.

Anodic and Cathodic UV-vis-NIR Spectroelectrochemistry

To further explore the reversible redox processes revealed by the CV of **1a**, **1b** and reference complex **1'**, UV-vis-NIR spectroelectrochemical experiments were conducted at 298 K in dichloromethane with an optically transparent thin-layer electrochemical (OTTLE) cell. Corresponding spectral changes are shown in Figures 5(a, b) and 6, and Figure S4.

The one-electron oxidation of complex **1'** to corresponding (di)cation **[1']**$^+$ did not

result in a substantial change in the UV-vis absorption (Figure 5(a)). Diagnostically it is important to note that (i) [**1'**]$^+$ does not absorb at all in the far red-NIR region, and (ii) only weak absorption appears in the course of the electrochemical oxidation of the metallacycle (see the next theoretical section) in the range of 21000-14000 cm^{-1}. According to the time-dependent (TD) DFT calculations (Table 4) the low-energy absorption of [**1'**]$^+$ is supposed to be more intense. The low conversion may be ascribed to working electrode passivation. In contrast, both DPA-substituted complexes **1a** and **1b** afford stable singly oxidized states characterized by absorption bands of a moderate intensity in the far red visible/NIR region. Figure 6 documents the twin absorption of [**1a**]$^+$ between 15000–10000 cm^{-1} that testifies to the formation of the DPA$^+$ moiety populated by the electronic excitation in this spectral region. The same qualitative reasoning applies for [**1b**]$^+$, prepared by both electrochemical (Figure S4) and chemical (Figure S5) oxidation, which shows a well-resolved absorption band at 12550 cm^{-1} encompassing several excitations directed into the β-LUSO localized dominantly on the oxidized methoxy-substituted DPA$^+$ group (Table 4).

The reductive UV-vis spectroelectrochemistry at ambient conditions was conducted only with **1'** that shows the reversible cathodic CV response (Figure 3). Passing the cathodic wave resulted in the transformation of the lowest-energy absorption band at 23950 cm^{-1} to a slightly blue-shifted broader band of a lower intensity (Figure 5b, Table 3). The same spectral change was observed when **1'** was swiftly reduced to [**1′**]$^-$ chemically with cobaltocene (Figure S6). The assignment of the new low-energy absorption is not trivial, with nearly the whole reduced metallacycle being involved, and requires support from theoretical calculations presented in the following section.

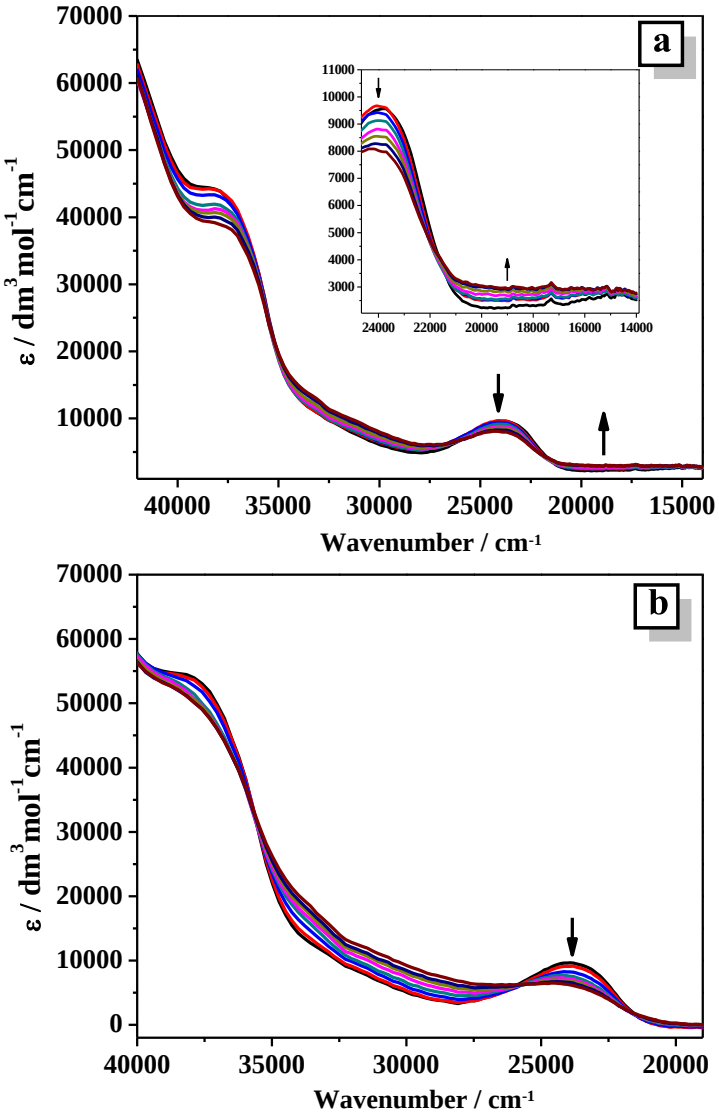

Figure 5. UV-vis spectral changes recorded during the oxidation (a) and reduction (b) of complex **1'** in CH_2Cl_2/*n*-Bu_4NPF_6 at 298 K within an OTTLE cell.

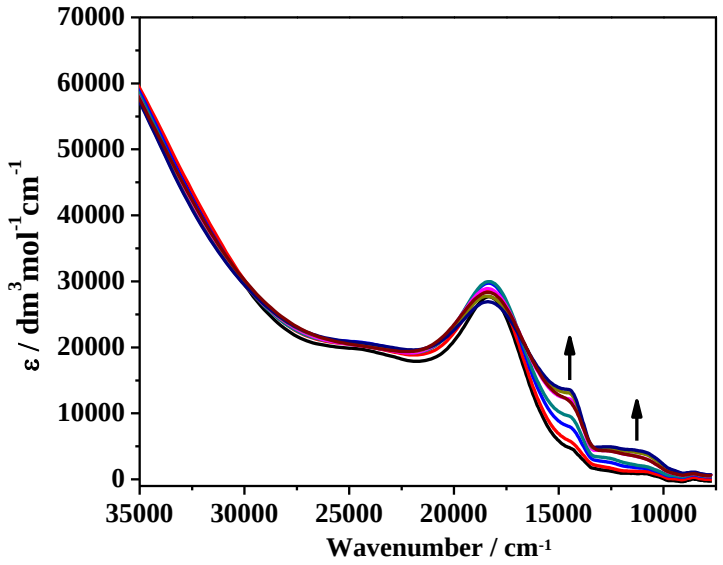

Figure 6. UV-vis-NIR spectral changes recorded during the oxidation of complex **1a** to [**1a**]$^{+}$ in $CH_2Cl_2/10^{-1}$ M *n*-Bu_4NPF_6 at 298 K within an OTTLE cell.

Theoretical Calculations

To facilitate accurate description of bonding and electronic properties of the studied osmanaphthalynes in the diverse redox states, DFT and TDDFT calculations on their optimized structures (B3LYP/6-31G*) were carried out. Optimized bond lengths and -angles have correlated well with the X-ray crystal structure data available for **1a** (Table 1), thereby proving the applicability of the chosen basis set and functional.

The geometry-optimized complexes **1a** and **1b** are showed in Figure S7. Modelled complex **1a** exhibita much shorter N–C bond (1.379 Å) linking DPA with the osmanaphthalyne metallacycle, compared to the other two N–C bonds in the DPA unit (1.437 Å and 1.440 Å), in agreement with the crystal data for **1a** (Table 1). These results indicate some conjugation between the osmanaphthalyne metallacycle and the DPA unit, affecting their oxidation potentials but not combining the two parts into a single redox-active unit, in line with the results of the preceding electrochemical study. For complex **1b**, the additional methoxy groups on DPA do not affect the three N–C bond lengths significantly (1.375 Å, 1.437 Å, 1.439 Å respectively). However, they affect strongly the anodic potentials by the push electron effect (Table 2).

The frontier orbitals, HOMOs and LUMOs, of **1'**, **1a** and **1b** are presented in the Figure 7. In the neutral state (neglecting the positive charge on the phosphonium substituent), the HOMOs of the complexes **1a** and **1b** are localized for a great deal on the DPA redox centers (51% and 67%, respectively). The Os center is underrepresented in the HOMO description, with only 5% contribution in **1b**. The spin density distribution of one-electron-oxidized $[\mathbf{1'}]^+$, $[\mathbf{1a}]^+$, $[\mathbf{1b}]^+$ is visualized in Figure 8. In reference radical $[\mathbf{1'}]^+$ lacking DPA, the spin density mainly resides on the Os center and the Os–Cl bonds most affected by the initial oxidation, as inferred from the combined experimental voltammetric and spectroelectrochemical results. In $[\mathbf{1a}]^+$ and $[\mathbf{1b}]^+$ the spin density resides largely on the DPA segment, with a minor involvement of the osmanaphthalyne metallacycles. Some π-interaction between DPA and the ligated osmium center mediated by the metallacycle backbone is apparent from the HOMOs of **1a** and **1b** (Figure 7). This contact opens chances for electronic excitation from the metallacycle (donor ligands on Os) to DPA^+ in both $[\mathbf{1a}]^+$ and $[\mathbf{1b}]^+$ (see below).

The localization of the one-electron reduction of complexes **1'**, **1a** and **1b** could not be judged convincingly by the analysis of their CV responses, and the cathodic SEC (for **1'**) data. The the spin density distribution in radicals $[\mathbf{1'}]^-$, $[\mathbf{1a}]^-$, $[\mathbf{1b}]^-$ has therefore been obtained from DFT calculations on their approved models, as visualized in Figure 9. In all three cases the spin density distribution in the singly-reduced states is very similar, involving the whole metallacycle with a only minor (< 5%) participation of the DPA p_π(N) site. These data have revealed that the osmanaphthalyne metallacycle plays a major role in the reduction process, which makes it possible to apprehend the corresponding UV-Vis spectroelectrochemical spectral changes (Figure 5(a)).

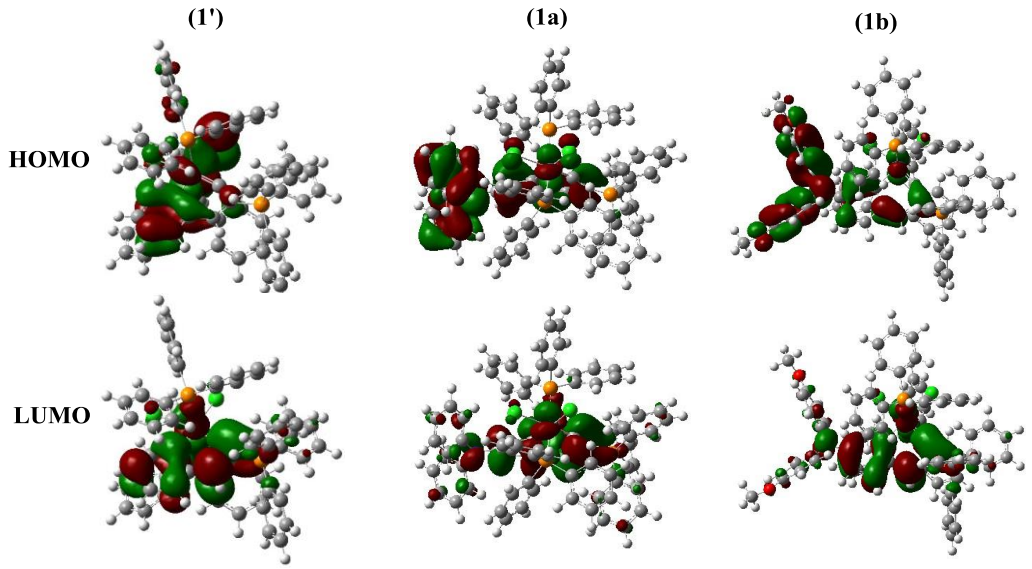

Figure 7. HOMOs and LUMOs molecular orbitals of complex **1'**, **1a**, **1b**. Contour values: ±0.02 $(e/bohr3)^{1/2}$. B3LYP/6-31G*(Os: Lanl2DZ) /CPCM /CH_2Cl_2.

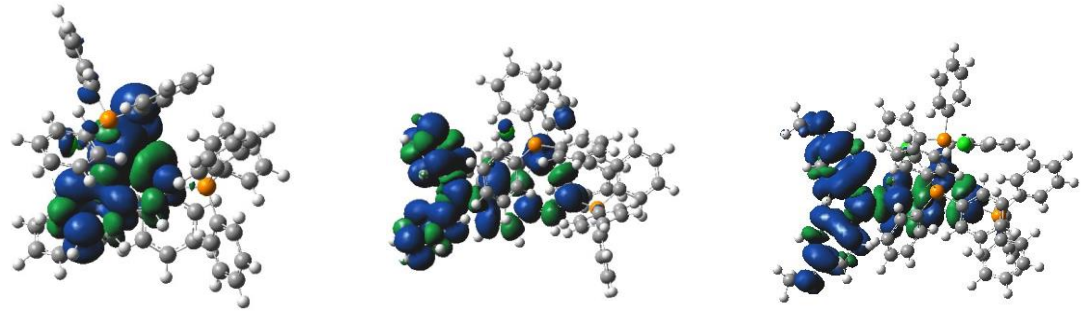

Figure 8. Calculated spin-density distribution in [**1'**]$^+$, [**1a**]$^+$, [**1b**]$^+$ Contour values: ±0.02 $(e/bohr3)^{1/2}$. B3LYP/6-31G*(Os: Lanl2DZ) /CPCM /CH_2Cl_2.

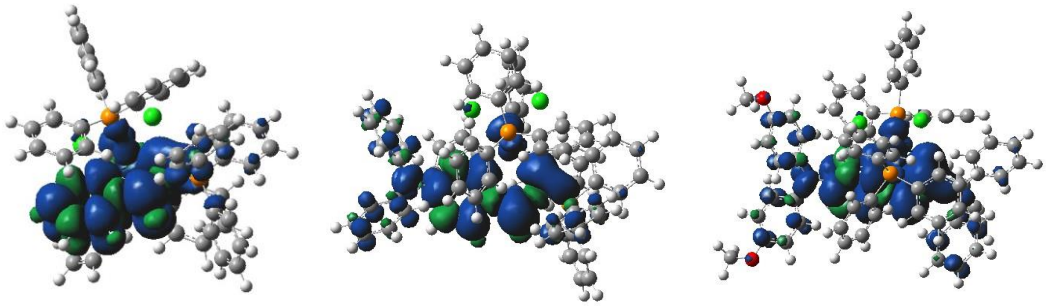

Figure 9. Calculated spin-density distribution in [**1'**]$^{-}$, [**1a**]$^{-}$, [**1b**]$^{-}$. Contour values: ±0.02 (e/bohr3)$^{1/2}$. B3LYP/6-31G*(Os: Lanl2DZ) /CPCM /CH_2Cl_2.

Finally, we briefly analyze the electronic absorption spectra in the studied osmanaphthalyne redox series with the aid of TDDFT calculations (conducted at the same level of theory for each species), focusing on **1'** and the effect of the DPA substituents on the nature of the low-energy optical excitation. The main relevant electronic transitions in [**1'**]^{n}, [**1a**]^{n} and [**1b**]^{n} (n = +1, 0 and −1) investigated with UV-vis-NIR SEC (Table 3) are presented in Table 4 and depicted in Figure 10.

The TDDFT results help to assign the main visible absorption of parent osmanaphtalynes at around 24000 cm^{-1} (**1'**) and 18000 cm^{-1} (**1a** and **1b**) to HOMO−7→LUMO (for **1'**) and HOMO→LUMO (for **1a** and **1b**) transitions. With reference to the composition of the contributing molecular orbitals, this means that compound **1'** undergoes a Cl^{-}/PPh_3→Os(metallacycle) charge transfer that changes for **1a** and **1b** to a DPA→Os(metallacycle) charge transfer.

The asymmetric broad absorptions of [**1a**]$^{+}$ and [**1b**]$^{+}$ in the far red-NIR region mainly belong to β-HOSO-9→β-LUSO (77%) and β-HOSO-6/β-HOSO-8→β-LUSO (69%) transitions, respectively. Both β-LUSO of compounds **1a** and **1b** are localized on the oxidized TPA^{+} units, while the β-HOSO-9 of **1a** and β-HOSO-6/β-HOSO-8 of **1b** are mainly localized on the Cl^{-} ligands, metallacycle and PPh_3 ligands bound to the Os center. Herewith, they both represent charge transfer from the osmanaphthalyne metallacycle and

Os-PPh_3 sites to the DPA^+ units. For oxidized reference compound $[\mathbf{1'}]^+$, there is a broad and weak electronic absorption between 20000-15000 cm^{-1}. Based on the theoretical calculations, this optical excitation can be attributed to β-HOSO-18→β-LUSO (52%) featuring a PPh_3/Cl→$Os(C\hat{}C)^+$ charge transfer character.

The original low-energy absorption of **1'** at 23950 cm^{-1} gradually decreased upon the one-electron reduction (Figure 5(b)) and became replaced by a new, only slightly shifted and less intense absorption of $[\mathbf{1'}]^-$ at 24100 cm^{-1}. This energetic position was reproduced by TDDFT calculations for an electronic excitation shown to involve the most significant β-HOSO-1→β-LUSO (33%) component. Based on this credible result the lowest-energy absorption of $[\mathbf{1'}]^-$ can be attributed a π(ClOs≡CC)→PPh_3^+ charge transfer character.

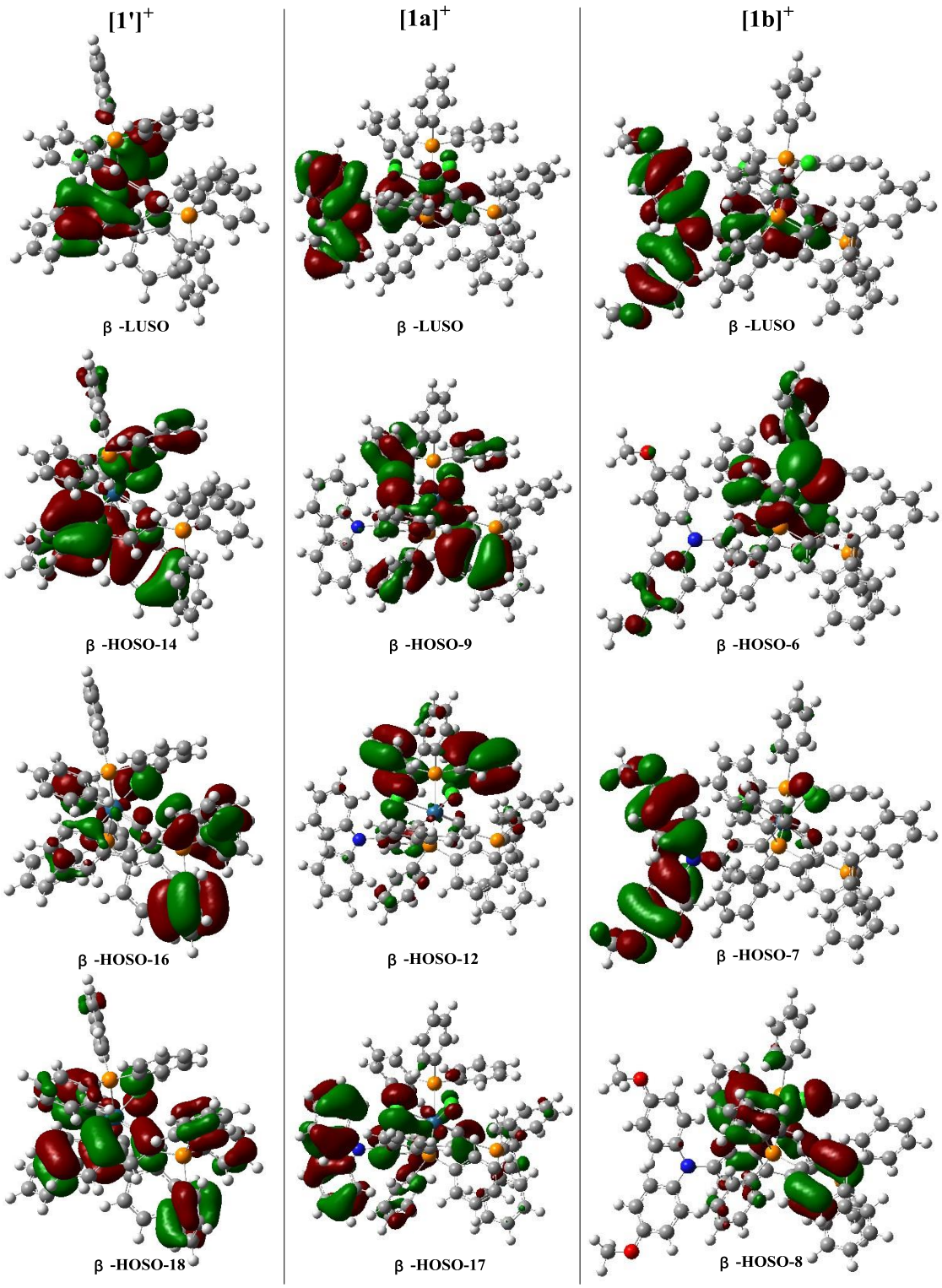

Figure 10. Spin orbitals involved in the major electronic excitations in [**1'**]$^+$ (left), [**1a**]$^+$ (middle) and [**1b**]$^+$ (right) presented in Table 4. B3LYP/6-31G* (Os:Lanl2DZ) /CPCM/CH_2Cl_2.

Table 4. Major electronic excitations in [**1'**]$^+$, [**1a**]$^+$ and [**1b**]$^+$ determined by the TD-DFT method.[a]

Complex	Excited State	λ (nm) [$\tilde{\nu}$ (cm^{-1})]	Osc. Strength (f)	Major Contributions	Assignment	$\tilde{\nu}$ (cm^{-1}) (experiment)
[1']	D_9	408 [24500]	0.04	HOMO-7→LUMO (79%)	Cl^-/PPh_3→Os(C^C)	**23950**
[1']$^-$	D_{25}	415 [24100]	0.02	β-HOSO-1→β-LUSO (33%)	π(ClOs≡CC)→PPh_3^+	**24100**
[1']$^+$	D_{17}	656 [15250]	0.02	β-HOSO-18→β-LUSO (52%) β-HOSO-16→β-LUSO (20%) β-HOSO-14→β-LUSO (18%)	PPh_3→Os(C^C)$^+$ Cl^-→Os(C^C)$^+$	**21000-14000 unresolved**
[1a]	D_2	518 [19300]	0.41	HOMO→LUMO (95%)	DPA→Os(metallacycle)	**18300**
[1a]$^+$	D_9	907 [11000]	0.03	β-HOSO-9→β-LUSO (77%) β-HOSO-11→β-LUSO (12%)	ClOs(C^C)/PPh_3→DPA^+	**11400**
	D_{13}	771 [13000]	0.02	β-HOSO-12→β-LUSO (32%) β-HOSO-14→β-LUSO (19%)	Os(C^C)/PPh_3→DPA^+	
	D_{20}	648 [15450]	0.04	β-HOSO-17→β-LUSO (22%)	DPA^+ (intraligand) Cl^-→DPA^+	**14450**
[1b]	D_2	564 [17750]	0.30	HOMO→LUMO (64%)	DPA→Os(metallacycle)	**18100**
[1b]$^+$	D_8	773 [12950]	0.03	β-HOSO-6→β-LUSO (19%) β-HOSO-8→β-LUSO (50%)	ClOs(C^C)/PPh_3→DPA^+	**12550**

	D_9	759 [13200]	0.10	β-HOSO-7→β-LUSO (59%) β-HOSO-8→β-LUSO (21%)	DPA^+ (intraligand) $ClOs(C^C)\rightarrow DPA^+$
	D_{15}	647 [15450]	0.02	β-HOSO-12→β-LUSO (18%) β-HOSO-13→β-LUSO (18%)	$Os(C^C)/PPh_3\rightarrow DPA^+$

[a]The DFT method was B3LYP/6-31G* (Os: Lanl2DZ) /CPCM/CH_2Cl_2.

Conclusions

In summary, we have described the syntheses, crystal structures, spectroscopic and redox properties of highly stable diphenylamine (DPA)-substituted osmanaphthalyne complexes **1a** and **1b** of a D-B-A-type, where the Os and DPA centers are linked by the backbone of the osmanaphthalyne metallacycle. The experimental results supported by theoretical calculations, unveiled the DPA redox site to oxidize prior to the oxidation of the metallacycle encountered for bare reference **1'**. Charge transfers to DPA^+ from the π-donor chlorido ligands and the Os(metallacycle) introduce new absorption in the far red-NIR spectral region, which may be further explored for application in optical materials. The metallacycle is also reducible but the donor DPA appendices compromise the stability of the radical anionic products. In general, electronic delocalization between the donor DPA and acceptor Os(metallacycle) moieties is limited. Direct electronic communication between these redox centres is evident from the strong donor-to-acceptor charge-transfer absorption in the visible spectral region. Variation of ligands in the Os coordination sphere and substituents at the metallacycle is assumed to have a huge impact on both redox and electronic absorption properties of these systems, and investigations along this research line have been in progress.

Experimental Section

***General Materials*.** Manipulations were carried out under an atmosphere of dry argon by using standard Schlenk techniques, unless stated otherwise. Solvents were dried by recommended procedures and distilled under an inert atmosphere prior to use. The starting materials 4-(diphenylamino)benzaldehyde (**4a**)[36] and 4-(bis(4-methoxyphenyl)amino)benzaldehyde (**4b**)[37], and reference osmanapthalyne complex **1′** (ref.[27]) were prepared by procedures described in the literature. Other reagents, and ferrocene, decamethylferrocene and cobaltocene used in the electrochemical studies, were received from commercial suppliers and used without further purification. Thianthrenium hexafluorophosphate ($TAPF_6$) used for the chemical oxidation of **1b**, was prepared by a published procedure.[38]

Syntheses. *Preparation of **3a**.* 4-(diphenylamino)benzaldehyde (**4a**) (4 g, 14.6 mmol) was dissolved in THF (100 mL) under argon and cooled down to 0 °C. In the following step, 0.5 M ethynylmagnesium bromide in tetrahydrofuran (33 mL, 16 mmol) was added to the reaction mixture that was then warmed up to room temperature. After standing for 4 h, the reaction mixture was quenched with a saturated aqueous solution of ammonium chloride and extracted with ethyl acetate. The combined organic extracts were dried upon anhydrous sodium sulfate, filtered, and concentrated in vacuo to obtain the crude product that was purified by column chromatography (eluent: petroleum ether/ethyl acetate, 10/1 (v/v)). Product **3a** was obtained as a yellow solid. Yield: 3.9 g (90%). ^{1}H NMR (600 MHz, $CDCl_3$; Figure S14): δ 7.39-7.41 (d, J = 12 Hz, 2H, Ar-H), 7.23-7.26 (t, J = 18 Hz, 4H, Ar-H), 7.06-7.09 (t, J = 18 Hz, 6H, Ar-H), 7.01-7.03 (t, J = 12 Hz, 2H, Ar-H), 5.40 (d, J = 6 Hz, 1H, ArCHOH), 2.66 (d, J = 6 Hz, 1H, CCH), 2.27 (s, 1H, OH). ^{13}C NMR (150 MHz, $CDCl_3$; Figure S15): δ 147.9, 147.3, 133.6, 129.1, 127.6, 124.3, 123.2, 122.9 (Ar), 83.6, 83.5 (CCH), 63.7 (ArCHOH). EI-MS (Figure S8): *m/z*: 299.02 $[M]^+$; calculated exact mass:

299.13. Anal. Calcd (%) for $C_{21}H_{17}NO$: C, 84.25; H, 5.72; N, 4.68. Found: C, 84.23; H, 5.70; N, 4.66.

*Preparation of **2a***. Complex **3a** (1.03 g, 3.44 mmol) was added under argon to a solution of $[OsCl_2(PPh_3)_3]$ (3 g, 2.86 mmol) in THF (20 mL),. The reaction mixture was stirred for 6 h at room temperature to give a yellow-brown solution. Diethyl ether (80 mL) was then added to the solution to induce precipitation. A deep-yellow precipitate was collected by filtration, washed with diethyl ether (3 × 50 mL), and dried under vacuum to give a yellow solid (2.78 g, 72%). Still under argon, a suspension of the yellow solid in methanol (20 mL) was treated with $HBF_4 \cdot Et_2O$ (0.48 mL, 3.2 mmol) and heated to reflux for about 3 h. Cooling down the reaction mixture afterwards to ambient temperature led to separation of deep purple solid **2a** that was collected by filtration, washed by methanol and dried under vacuum. Yield: 1.5 g (51%). ^{1}H NMR (600 MHz, $CDCl_3$; Figure S18): δ 9.69 (s, 1H, OsCC(PPh_3)CH), 6.60-7.75 (m, 60H, other aromatic protons), -6.21 (t, J = 30 Hz, 1H, OsH). ^{31}P NMR (160 MHz, $CDCl_3$; Figure S19): δ 16.7 ($OsPPh_3$), 4.1 ($CPPh_3$). ^{13}C NMR (150 MHz, $CDCl_3$; Figure S20): δ 252.6 (Os≡C), 155.2, 154.6, 154.5, 143.7, 140.3, 140.3, 136.9, 136.7, 135.4, 134.4, 132.7, 132.5, 132.3, 130.2, 130.0, 129.9, 127.7, 127.3, 126.7, 125.4, 125.3, 119.7, 117.5, 117.3, 116.7, 115.1, 114.5 (other aromatic carbon atoms). HRMS (ESI): *m/z* calcd for $[C_{75}H_{61}Cl_2NOsP_3]^+$, 1330.3009; found: 1330.2973 (Figure S11). Anal. Calcd (%) for $C_{75}H_{61}BCl_2F_4NOsP_3$: C, 63.56; H, 4.34; N, 0.99. Found: C, 63.75; H, 4.57; N, 1.05.

*Preparation of **1a***. Complex **2a** (200 mg, 0.14 mmol) was dissolved in 1,2-dichloroethane (5 mL). The solution was heated to reflux for 12 h under an O_2 atmosphere and cooled afterwards to ambient temperature. The solvent was evaporated under vacuum to reduce the solution volume to ca 2 mL. Subsequent addition of diethyl ether (15 mL) led to separation of deep purple solid **1a** that was collected by filtration, washed by methanol and dried in vacuo. Yield: 141 mg (71%). ^{1}H NMR (400 MHz, $CDCl_3$; Figure S24): δ 7.76 (t, J = 6.8 Hz, 4H), 7.68–7.54 (m, 7H), 7.42 (dd, J = 12.4, 5.4 Hz, 13H), 7.28 – 7.09 (m,

19H), 6.98 (t, J = 7.5 Hz, 12H), 6.63 (s, 3H), 6.35 (dd, J = 9.1, 2.4 Hz, 1H). ^{31}P NMR (160 MHz, $CDCl_3$; Figure S25): δ 12.3 ($OsPPh_3$), -7.9 ($CPPh_3$). ^{13}C NMR (100 MHz, $CDCl_3$; Figure S26): δ 267.9 (Os≡C), 175.5, 164.5, 153.2, 146.2, 143.1, 135.1, 134.7, 134.0, 132.2, 132.1, 132.0, 131.7, 131.5, 131.2, 130.7, 130.6, 130.5, 129.9, 129.5, 128.6, 128.5, 127.7, 127.6, 127.6, 126.9, 126.29, 122.4, 119.9, 119.0, 112.3, 112.2, 112.2, 94.4, 93.2 (other aromatic carbon atoms). HRMS (ESI): *m/z* calcd for $[C_{75}H_{59}Cl_2NOsP_3]^+$, 1328.2852; found: 1328.2761 (Figure S10). Anal. Calcd (%) for $C_{75}H_{59}BCl_2F_4NOsP_3$: C, 63.66; H, 4.20; N, 0.99. Found: C, 63.43; H, 4.32; N, 1.03.

*Preparation of **3b.*** 4-(bis(4-methoxyphenyl)amino)benzaldehyde (**4b**) (4.4 g, 13.2 mmol) was dissolved under argon in tetrahydrofuran (100 mL) and cooled down to 0 °C. In the following step, 0.5 M ethynylmagnesium bromide in THF (30 mL, 15 mmol) was added to the reaction mixture that was then warmed up to room temperature. After standing for 4 h, the reaction mixture was quenched with a saturated aqueous solution of ammonium chloride and extracted with ethyl acetate. The combined organic extracts were dried with anhydrous sodium sulfate, filtered, and concentrated in vacuo to obtain the crude product that was purified by column chromatography (eluent: petroleum ether/ethyl acetate, 5/1 (v/v)). Product **3b** was obtained as a yellow oil. Yield: 4.2 g (89%). ^{1}H NMR (400 MHz, $CDCl_3$; Figure S14): δ 7.32-7.35 (d, J = 12 Hz, 2H, Ar-H), 7.03-7.07 (m, 4H, Ar-H), 6.90-6.92 (m, 2H, Ar-H), 6.81-6.85 (m, 4H, Ar-H), 5.38 (dd, J_1 = 2 Hz, J_2 = 2 Hz, 1H, ArCHOH), 3.80 (s, 6H, OCH_3), 2.66 (d, J = 2.2 Hz, 1H, CCH), 2.12-2.14 (d, J = 8 Hz, 1H, OH). ^{13}C NMR (150 MHz, $CDCl_3$; Figure S15): δ 155.4, 148.5, 140.4, 131.7, 127.4, 126.2, 119.9, 114.4 (Ar), 83.8 (CCH), 74.2 (CCH), 63.4 (ArCHOH), 55.1 (OCH_3). EI-MS: *m/z*: 359.06 $[M]^+$; calculated exact mass: 359.15 (Figure S9). Anal. Calcd (%) for $C_{23}H_{21}NO_3$: C, 76.86; H, 5.89; N, 3.90. Found: C, 76.85; H, 5.86; N, 3.94.

*Preparation of **2b.*** Complex **3b** (2.22 g, 6.18 mmol) was added under argon to a solution of $[OsCl_2(PPh_3)_3]$ (5.4 g, 5.15 mmol) in THF (30 mL),. The reaction mixture was stirred for 6 h at room temperature to give a brown solution. Subsequent addition of diethyl

ether (80 mL) to the solution gave a deep yellow precipitate that was collected by filtration, washed with diethyl ether (3 × 50 mL) and dried under vacuum to give a deep yellow solid. Yield 5 g (70%). Still under argon, a suspension of the deep yellow solid in methanol (30 mL) was treated with $HBF_4 \cdot Et_2O$ (0.82 mL, 5.5 mmol) and then heated to reflux for ca 3 h. Cooling down the reaction mixture afterwards to ambient temperature led to separation of dark blue solid **2b** that was collected by filtration, washed by methanol and dried in vacuo. Yield: 2.78 g (53%). ^{1}H NMR (400 MHz, $CDCl_3$; Figure S21): δ 9.68-9.66 (d, *J* = 8 Hz, 1H, OsCC(PPh_3)CH), 7.78-7.71 (m, 5H), 7.50-7.37 (m, 30H), 7.20-7.13 (m, 14H), 6.94 (d, *J* = 8.6 Hz, 5H), 6.64-6.59 (m, 5H), 3.85 (s, 6H), -6.27 (td, *J* = 15.2, 2.8 Hz, 1H). ^{31}P NMR (160 MHz, $CDCl_3$; Figure S22): δ 18.01 ($OsPPh_3$), 5.78 ($CPPh_3$). ^{13}C NMR (100 MHz, $CDCl_3$; Figure S23): δ 253.6 (Os≡C), 158.8, 158.2, 157.8, 156.1, 154.2, 141.0, 137.4, 136.7, 135.4-132.0, 130.4, 130.1, 130.0, 129.9, 129.7, 128.6-127.5, 126.2, 125.3, 122.2, 119.1, 118.1, 117.2, 116.9, 115.5, 115.1-114.7, 113.8, 113.0 (other aromatic carbon atoms), 55.6, 55.6 (OCH_3). HRMS (ESI): *m/z* calcd for $[C_{77}H_{65}Cl_2NO_2OsP_3]^+$, 1390.3220; found: 1390.3176 (Figure S13). Anal. Calcd (%) for $C_{77}H_{65}BCl_2F_4NO_2OsP_3$: C, 62.61; H, 4.44; N, 0.95. Found: C, 62.96; H, 4.60; N, 1.12.

*Preparation of **1b.*** Complex **2b** (200 mg, 0.135 mmol) was dissolved in 1,2-dichloroethane (5 mL) and heated to reflux for 12 h under an O_2 atmosphere. The reaction mixture was then cooled down to ambient temperature and the solvent was evaporated under vacuum to reduce the volume to ca 2 mL. Subsequent addition of diethyl ether (30 mL) to the solution led to separation of deep purple solid **1b** that was collected by filtration, washed three times with diethyl ether and dried in vacuo. Yield: 140 mg (70%). ^{1}H NMR (400 MHz, $CDCl_3$; Figure S27): δ 7.76-6.25 (m, 57H, other aromatic protons), 3.80 (s, 6H, OCH_3). ^{31}P NMR (160 MHz, $CDCl_3$; Figure S28): δ 12.08 ($OsPPh_3$), -7.93 ($CPPh_3$). ^{13}C NMR (100 MHz, CD_3CN; Figure S29): δ 269.2 (Os≡C), 176.3, 167.4, 162.6, 162.5, 159.4, 158.0, 156.3, 154.9, 145.4, 141.7, 140.0, 139.6, 137.1-134.3, 132.5-128.5, 127.4-119.8, 116.3-115.3, 111.8, 94.3, 93.2 (other aromatic carbon atoms), 56.3, 56.2 (OCH_3). HRMS

(ESI): *m/z* calcd for $[C_{77}H_{63}Cl_2NO_2OsP_3]^+$, 1388.3063; found: 1388.3054 (Figure S12). Anal. Calcd (%) for $C_{77}H_{65}BCl_2F_4NO_2OsP_3$: C, 62.69; H, 4.30; N, 0.95. Found: C, 62.30; H, 4.58; N, 1.13.

Crystallographic Details

Single crystals of complexes **1a** and **2a** suitable for X-ray analysis were grown at room temperature by slow diffusion of hexane into a saturated solution in dichloromethane, and tetrahydrofuran into a saturated solution in dichloromethane, respectively. Crystals having approximate dimensions of 0.20 × 0.15 × 0.10 mm^3 for **1a** and 0.15 × 0.12 × 0.10 mm^3 for **2a** were mounted on a glass fiber for diffraction experiments. Intensity data for these crystals were collected at room temperature on a Nonius Kappa CCD diffractometer with Mo Kα radiation (0.71073 Å). The structures were solved by SHELXS-97[39] and Fourier difference techniques, and refined by SHELXL-2014.[40] Crystal data for **1a** and **2a** and details of the data collection are summarized in Table S1. Selected bond distances and angles in **1a** and **2a** are given in Tables S2 and S3, respectively. The CCDC numbers for **1a** and **2a** are 1841463 and 1841462, respectively.

Physical Measurements

^1H, ^{13}C, and ^{31}P NMR spectra were collected on Varian Mercury Plus 400 (400 MHz) or Varian Mercury Plus (600 MHz) spectrometers. ^1H and ^{13}C NMR chemical shifts are given relative to TMS, and ^{31}P NMR chemical shifts relative to 85% H_3PO_4. Elemental analyses (C, H, N) were performed with an Elementar Vario EL III instrument. The high-resolution mass spectra (HRMS) were recorded on a Thermo Exactive plus mass spectrometer. Electrochemical measurements were carried out with a CHI 660C potentiostat. The analyte and supporting electrolyte (*n*-Bu_4NPF_6) concentrations were 10^{-3} and 10^{-1} mol dm^{-3}, respectively, in dry argon-saturated dichloromethane (or acetonitrile for **1a**). The air-tight single-compartment cell for cyclic voltammetry and Osteryoung

square-wave voltammetry contained a d = 0.5 mm platinum disk working electrode (pre-polished carefully with 0.25-μm diamond paste), a coiled platinum wire counter electrode, and a coiled Ag wire electrode. Ferrocene and decamethylferrocene were added as internal potential standards. Spectroelectrochemical experiments were carried out at room temperature with an optically transparent thin-layer electrochemical (OTTLE) cell (optical path length of ca. 200 μm) equipped with a Pt minigrid working electrode and CaF_2 windows.[41] The OTTLE cell was placed in the sample compartment of a Shimadzu UV-3600 UV-vis-NIR spectrophotometer. The controlled-potential electrolyses were conducted with a CHI 660C potentiostat. The concentrations of the analyte and supporting electrolyte (n-Bu_4NPF_6) were ca. 2×10^{-3} mol dm^{-3} and 3×10^{-1} mol dm^{-3}, respectively.

Computational Details

DFT calculations were performed with the Gaussian 09 program[42] at the B3LYP[43]/6-31G* (Lanl2DZ for the osmium atom) levels of theory. Geometry optimization was performed without any symmetry constraints. The MO contributions were generated by using the Multiwfn2.6.1_bin_Win package, and plotted by GaussView 5.0 and the electronic transitions were calculated by the method of TD-DFT. The solvation effects in dichloromethane were simulated by having employed the conductor-like polarizable continuum model (CPCM).[44]

Acknowledgements

The authors gratefully acknowledge financial support from National Natural Science Foundation of China (21472059, 21772054), and the 111 Project (B17019).

Author Information

Corresponding Authors:

E-mail: chshliu@mail.ccnu.edu.cn

E-mail: f.hartl@reading.ac.uk

ORCID

František Hartl: 0000-0002-7013-5360

Notes

The authors declare no competing financial interest.

† **Electronic supplementary information (ESI) available:** Crystallographic details, complementary cyclic and square wave voltammograms, EI-MS, ESI-MS and NMR spectra, complementary UV-vis-NIR absorption spectra, solvatochromism of **1a**, DFT optimized geometries of **1a**, **1b**, and **2a**.

References

[1] Thorn, D. L.; Hoffmann, R. Delocalization in metallocycles. *Nouv. J. Chim*. **1979**, *3*, 39-45.

[2] Elliott, G. P.; Roper, W. R.; Waters, J. M. Metallacyclohexatrienes or 'metallabenzenes.' Synthesis of osmabenzene derivatives and X-ray crystal structure of [Os(CSCHCHCHCH)(CO)(PPh_3)$_2$]. *J. Chem. Soc., Chem. Commun*., **1982**, 811-813.

[3] (a) Bleeke, J. R. Metallabenzene chemistry. *Acc. Chem. Res.* **1991**, *24*, 271-277; (b) Bleeke, J. R. Metallabenzenes. *Chem. Rev*. **2001**, *101*, 1205-1227; (c) He, G.; Xia, H.; Jia, G. Progress in the synthesis and reactivity studies of metallabenzenes. *Chin. Sci. Bull*. **2004**, *49*, 1543-1553; (d) Landorf, C. W.; Haley, M. M. Recent Advances in Metallabenzene Chemistry. *Angew Chem. Int. Ed*. **2006**, *45*, 3914-3936; (e) Bleeke, J. R. Aromatic Iridacycles. *Acc. Chem. Res*. **2007**, *40*, 1035-1047; (f) Xia, H.; He, G.; Zhang, H.; Wen, T. B.; Sung, H. H. Y.; Williams, I. D.; Jia, G. Osmabenzenes from the Reactions of HC≡CCH(OH)C≡CH with $OsX_2(PPh_3)_3$ (X = Cl, Br). *J. Am. Chem. Soc*. **2004**, *126*, 6862-6863; (g) Zhang, H.; Xia, H.; He, G.; Wen, T. B.; Gong, L.; Jia, G. Synthesis and Characterization of Stable

Ruthenabenzenes. *Angew. Chem. Int. Ed*. **2006**, *45*, 2920-2923; (h) Poon, K. C.; Liu, L.; Guo, T.; Li, J.; Sung, H. H. Y.; Williams, I. D.; Lin, Z.; Jia, G. Synthesis and Characterization of Rhenabenzenes. *Angew. Chem. Int. Ed*. **2010**, *49*, 2759-2762; (i) Han, F.; Li, J.; Zhang, H.; Wang, T.; Lin, Z.; Xia, H. Reactions of Osmabenzene with Silver/Copper Acetylides: From Metallabenzene to Benzene. *Chem. Eur. J*. **2015**, *21*, 565-567.

[4] (a) DeShong, P.; Sidler, D. R.; Rybczynski, P. J.; Slough, G. A.; Rheingold, A. L. A general method for the preparation of carbonyl compounds and butenolides from organomanganese pentacarbonyl complexes. *J. Am. Chem. Soc*. **1988**, *110*, 2575-2585; (b) Komiya, S.; Ito, T.; Cowie, M.; Yamamoto, A.; Ibers, J. A. Carbon-hydrogen bond activation by transition metal complexes. Oxidative addition of alkyl methacrylate to ruthenium. The structure of hydrido(2-n-butoxycarbonylpropenyl-C1,O)tris(triphenylphosphine)ruthenium(II). *J. Am. Chem. Soc*. **1976**, *98*, 3874-3884; (c) Padolik, L. L.; Galluci, J. C.; Wojcicki, A. Fischer-type rhenacyclobutadiene complexes: synthesis, structure, and nucleophilic addition/substitution and oxidation reactions. *J. Am. Chem. Soc*. **1993**, *115*, 9986-9996; (d) Garrett, K. E.; Sheridan, J. B.; Pourreau, D. B.; Feng, W. C.; Geoffroy, G. L.; Staley, D. L.; Rheingold, A. L. Transient generation of the reactive carbene complex $[Cp(CO)_2W{=}CH(Tol)]^+$ and its reactions with alkynes to form vinylcarbene, allyl, naphthol, diene, and metallafuran complexes. *J. Am. Chem. Soc*. **1989**, *111*, 8383-8391; (e) Grotjahn, D. B.; Hoerter, J. M.; Hubbard, J. L. Double C−H Activation during Functionalization of Phenyl(methyl)ketene on Iridium(I) Using Alkynes. Synthesis of 1, 4-Dien-3-ones. *J. Am. Chem. Soc*. **2004**, *126*, 8866-8867.

[5] (a) Wen, T. B.; Zhou, Z. Y.; Jia, G. Synthesis and Characterization of a Metallabenzyne. *Angew. Chem. Int. Ed*. **2001**, *40*, 1951-1954; (b) Wen, T. B.; Ng, S. M.; Hung, W. Y.; Zhou, Z. Y.; Lo, M. F.; Shek, L. Y.; Williams, I. D.; Lin, Z.; Jia,

G. Protonation and Bromination of an Osmabenzyne: Reactions Leading to the Formation of New Metallabenzynes. *J. Am. Chem. Soc*. **2003**, *125*, 884-885; (c) Jia, G. Progress in the Chemistry of Metallabenzynes. *Acc. Chem. Res*. **2004**, *37*, 479-486; (d) Wen, T. B.; Hung, W. Y.; Sung, H. H. Y.; Williams, I. D.; Jia, G. Syntheses of Metallabenzynes from an Allenylcarbene Complex. *J. Am. Chem. Soc*. **2005**, *127*, 2856-2857; (e) Hung, W. Y.; Zhu, J.; Wen, T. B.; Yu, K. P.; Sung, H. H.Y.; Williams, I. D.; Lin, Z.; Jia, G. Osmabenzenes from the Reactions of a Dicationic Osmabenzyne Complex. *J. Am. Chem. Soc*. **2006**, *128*, 13742-13752; (f) He, G.; Zhu, J.; Hung, W. Y.; Wen, T. B.; Sung, H. H. Y.; Williams, I. D.; Lin Z.; Jia, G. A Metallanaphthalyne Complex from Zinc Reduction of a Vinylcarbyne Complex. *Angew. Chem. Int. Ed*. **2007**, *46*, 9065-9068; (g) Hung, W. Y.; Liu, B.; Shou, W.; Wen, T. B.; Shi, C.; Sung, H. H. Y.; Williams, I. D.; Lin, Z.; Jia, G. Electrophilic Substitution Reactions of Metallabenzynes. *J. Am. Chem. Soc*. **2011**, *133*, 18350-18360; (h) Chen, J.; Sung, H. H. Y.; Williams, I. D.; Lin, Z.; Jia, G. Synthesis and Characterization of a Rhenabenzyne Complex. *Angew. Chem. Int. Ed.* **2011**, *50*, 10675-10678; (i) Jia, G. Our Journey to the Chemistry of Metallabenzynes. *Organometallics* **2013**, *32*, 6852-6866.

[6] Weller, K. J.; Filippov, I.; Briggs, P. M.; Wigley, D. E. Pyridine Degradation Intermediates as Models for Hydrodenitrogenation Catalysis: Preparation and Properties of a Metallapyridine Complex. *Organometallics* **1998**, *17*, 322-329.

[7] (a) Paneque, M.; Posadas, C. M.; Poveda, M. L.; Rendón, N.; Santos, L. L.; Álvarez, E.; Salazar, V.; Mereiter, K.; Oñate, E. Metallacycloheptatrienes of Iridium(III): Synthesis and Reactivity. *Organometallics* **2007**, *26*, 3403–3415; (b) Paneque, M.; Posadas, C. M.; Poveda, M. L.; Rendón, N.; Salazar, V.; Oñate, E.; Mereiter, K. Formation of Unusual Iridabenzene and Metallanaphthalene Containing Electron-Withdrawing Substituents. *J. Am. Chem. Soc*. **2003**, *125*, 9898–9899.

[8] He, G.; Zhu, J.; Hung, W. Y.; Wen, T. B.; Sung, H. H. Y.; Williams, I. D.; Lin, Z.;

Jia, G. A Metallanaphthalyne Complex from Zinc Reduction of a Vinylcarbyne Complex. *Angew. Chem. Int. Ed*. **2007**, *46*, 9065-9068.

[9] (a) Wang, T.; Han, F.; Huang, H.; Li, J.; Zhang, H.; Zhu, J.; Lin, Z.; Xia, H. Synthesis of Aromatic Aza-metallapentalenes from Metallabenzene via Sequential Ring Contraction/Annulation. *Scientific Reports* **2015**, *5,* 9584-9590; (b) Zhu, C.; Yang, Y.; Wu, J.; Luo, M.; Fan, J.; Zhu, J.; Xia, H. Five-Membered Cyclic Metal Carbyne: Synthesis of Osmapentalynes by the Reactions of Osmapentalene with Allene, Alkyne, and Alkene. *Angew. Chem. Int. Ed.* **2015**, *54*, 7189-7192; (c) Luo, M.; Zhu, C.; Chen, L.; Zhang, H.; Xia, H. Halogenation of carbyne complexes: isolation of unsaturated metallaiodirenium ion and metallabromirenium ion. *Chem. Sci*. **2016**, *7*, 1815-1818; (d) Zhu, C.; Li, S.; Luo, M.; Zhou, X.; Niu, Y.; Lin, M.; Zhu, J.; Cao, Z.; Lu, X.; Wen, T. B.; Xie, Z.; Schleyer, P. R.; Xia, H. Stabilization of anti-aromatic and strained five-membered rings with a transition metal. *Nat. Chem*. **2013**, *5*, 698–703.

[10] Zhuo, Q.; Zhang, H.; Hua, Y.; Kang, H.; Zhou, X.; Lin, X.; Chen, Z.; Lin, J.; Zhuo, K.; Xia, H. Constraint of a ruthenium-carbon triple bond to a five-membered ring. *Sci. Adv.* **2018**, *4*, in the press. DOI: 10.1126/sciadv.aat0336.

[11] (a) Clark, G. R.; Johns, P. M.; Roper, W. R.; Wright, L. J. A Stable Iridabenzene Formed from an Iridacyclopentadiene Where the Additional Ring-Carbon Atom Is Derived from a Thiocarbonyl Ligand. *Organometallics* **2008**, *27*, 451–454; (b) Wang, T.; Li, S.; Zhang, H.; Lin, R.; Han, F.; Lin, Y.; Wen, T. B.; Xia, H. Annulation of Metallabenzenes: From Osmabenzene to Osmabenzothiazole to Osmabenzoxazole. *Angew. Chem. Int. Ed*. **2009**, *48*, 6453–6456; (c) Clark, G. R.; Ferguson, L. A.; McIntosh, A. E.; Söhnel, T.; Wright, L. J. Functionalization of Metallabenzenes through Nucleophilic Aromatic Substitution of Hydrogen. *J. Am. Chem. Soc*. **2010**, *132*, 13443–13452; (d) Lin, R.; Zhang, H.; Li, S.; Wang, J.; Xia, H. New Highly Stable Metallabenzenes via Nucleophilic Aromatic Substitution

Reaction. *Chem. Eur. J*. **2011**, *17*, 4223–4231; (e) Wang, T.; Zhang, H.; Han, F.; Long, L.; Lin, Z.; Xia, H. Key Intermediates of Iodine-Mediated Electrophilic Cyclization: Isolation and Characterization in an Osmabenzene System. *Angew. Chem. Int. Ed*. **2013**, *52*, 9251-9255; (f) Paneque, M.; Posadas, C. M.; Poveda, M. L.; Rendón, N.; Santos, L. L.; Álvarez, E.; Salazar, V.; Mereiter, K.; Oñate, E. Metallacycloheptatrienes of Iridium(III): Synthesis and Reactivity. *Organometallics* **2007**, *26*, 3403–3415; (g) Bleeke, J. R.; Behm, R.; Xie, Y. F.; Chiang, M. Y.; Robinson, K. D.; Beatty, A. M. Synthesis, Structure, Spectroscopy, and Reactivity of a Metallabenzene. *Organometallics* **1997**, *16*, 606-623; (h) Bleeke, J. R.; Behm, R.; Xie, Y.-F.; Jr, T. W. C.; Robinson, K. D. Metallacyclohexadiene and Metallabenzene Chemistry. 10. Cycloaddition Reactions of a Metallabenzene. *J. Am. Chem. Soc*. **1994**, *116*, 4093–4094; (i) Bierstedt, A.; Clark, G. R.; Roper, W. R.; Wright, L. J. A 2-iridafuran from reaction between a 1-iridaindene and methyl propiolate. *J. Organomet. Chem.* **2006**, *691*, 3846-3852.

[12] (a) Wang, T.; Li, S.; Zhang, H.; Lin, R.; Han, F.; Lin, Y.; Wen, T. B.; Xia, H. Annulation of Metallabenzenes: From Osmabenzene to Osmabenzothiazole to Osmabenzoxazole. *Angew. Chem. Int. Ed*. **2009**, *48*, 6453–6456; (b) Lin, R.; Zhang, H.; Li, S.; Chen, L.; Zhang, W.; Wen, T. B.; Zhang, H.; Xia, H. pH-Switchable Inversion of the Metal-Centered Chirality of Metallabenzenes: Opposite Stereodynamics in Reactions of Ruthenabenzene with L- and D-Cysteine. *Chem. Eur. J*. **2011**, *17*, 2420–2427; (c) Zhu, C.; Zhu, Q.; Fan, J.; Zhu, J.; He, X.; Cao, X. Y.; Xia, H. A Metal-Bridged Tricyclic Aromatic System: Synthesis of Osmium Polycyclic Aromatic Complexes. *Angew. Chem. Int. Ed*. **2014***, 53,* 6232-6236.

[13] Liu, B.; Wang, H.; Xie, H.; Zeng, B.; Chen, J.; Tao, J.; Wen, T. B.; Cao, Z.; Xia, H. Osmapyridine and Osmapyridinium from a Formal [4+2] Cycloaddition Reaction. *Angew. Chem. Int. Ed*. **2009**, *48*, 5430-5434.

[14] (a) Zhang, H.; Wu, L.; Lin, R.; Zhao, Q.; He, G.; Yang, F.; Wen, T. B.; Xia, H.

Synthesis, Characterization and Electrochemical Properties of Stable Osmabenzenes Containing PPh_3 Substituents. *Chem. Eur. J*. **2009**, *15*, 3546 – 3559; (b) Huang, J.; Lin, R.; Wu, L.; Zhao, Q.; Zhu, C.; Wen, T. B.; Xia, H. Synthesis, Characterization, and Electrochemical Properties of Bisosmabenzenes Bridged by Diisocyanides. *Organometallics* **2010**, *29*, 2916-2925.

[15] (a) Low, P. J.; Brown, N. J. Electronic Interactions Between and Through Covalently-Bonded Polymetallic Complexes. *J. Cluster Sci*. **2010**, *21*, 235-278; (b) Kubiak, C. P. Inorganic Electron Transfer: Sharpening a Fuzzy Border in Mixed Valency and Extending Mixed Valency across Supramolecular Systems. *Inorg. Chem*. **2013**, *52*, 5663-5676; (c) Rosokha, S. V.; Kochi, J. K. Fresh Look at Electron-Transfer Mechanisms via the Donor/Acceptor Bindings in the Critical Encounter Complex. *Acc. Chem. Res*. **2008**, *41*, 641-653; (d) Hankache, J.; Wenger, O. S. Organic Mixed Valence. *Chem. Rev*. **2011**, *111*, 5138-5178; (e) Pieslinger, G. E.; Alborés, P.; Slep, L. D.; Baraldo, L. M. Class III Delocalization in a Cyanide-Bridged Trimetallic Mixed-Valence Complex. *Angew. Chem. Int. Ed*. **2014**, *53*, 1293-1296.

[16] (a) D'Alessandro, D. M.; Keene, F. R. Intervalence Charge Transfer (IVCT) in Trinuclear and Tetranuclear Complexes of Iron, Ruthenium, and Osmium. *Chem. Rev.* **2006**, *106*, 2270-2298; (b) Kaim, W.; Lahiri, G. K. Unconventional Mixed-Valent Complexes of Ruthenium and Osmium. *Angew. Chem. Int. Ed*. **2007**, *46*, 1778-1796; (c) Aguirre-Etcheverry, P.; O'Hare, D. Electronic Communication through Unsaturated Hydrocarbon Bridges in Homobimetallic Organometallic Complexes. *Chem. Rev*. **2010**, *110*, 4839-4864; (d) Yao, C. J.; Sui, L. Z.; Xie, H. Y.; Xiao, W. J.; Zhong, Y. W.; Yao, J. Electronic Coupling between Two Cyclometalated Ruthenium Centers Bridged by 1,3,6,8-Tetra(2-pyridyl)pyrene (tppyr). *Inorg. Chem*. **2010**, *49*, 8347-8350; (e) Wang, L.; Yang, W. W.; Zheng, R. H.; Shi, Q.; Zhong, Y. W.; Yao, J. Electronic Coupling between Two Cyclometalated

Ruthenium Centers Bridged by 1,3,6,8-Tetrakis(1-butyl-1H-1,2,3-triazol-4-yl)pyrene. *Inorg. Chem*. **2011**, *50*, 7074-7079.

[17] (a) Launay, J.-P. Electron transfer in molecular binuclear complexes and relation with electron transport through nanojunctions. *Coord. Chem. Rev*. **2013**, *257*, 1544-1554; (b) Sakamoto, R.; Katagiri, S.; Maeda, H.; Nishihara, H. Bis(terpyridine) metal complex wires: Excellent long-range electron transfer ability and controllable intrawire redox conduction on silicon electrode. *Coord. Chem. Rev.* **2013**, *257*, 1493-1506.

[18] Terada, K.; Kanaizuka, K.; Iyer, V. M.; Sannodo, M.; Saito, S.; Kobayashi, K.; Haga, M.-a. Memory Effects in Molecular Films of Free-Standing Rod-Shaped Ruthenium Complexes on an Electrode. *Angew. Chem. Int. Ed*. **2011**, *50*, 6287-6291.

[19] Kurata, T.; Koshika, K.; Kato, F.; Kido, J.; Nishide, H. An unpaired electron-based hole-transporting molecule: Triarylamine-combined nitroxide radicals. *Chem. Commun*. **2007**, 2986-2988.

[20] (a) Yin, J.-F.; Velayudham, M.; Bhattacharya, D.; Lin, H.-C.; Lu, K.-L. Structure optimization of ruthenium photosensitizers for efficient dye-sensitized solar cells – A goal toward a "bright" future. *Coord. Chem. Rev*. **2012**, *256*, 3008-3035; (b) Bomben. P. G.; Robson. K. C. D.; Koivisto. B. D.; Berlinguette, C. P. Cyclometalated ruthenium chromophores for the dye-sensitized solar cell. *Coord. Chem. Rev*. **2012**, *256*, 1438-1450.

[21] Liu, B.; Guo, C. L.; Liu, W. X.; Guo, M. E.; Yan, F.; Xue, L. S.; Wang, H. J.; Liu, C. L.; Jin, S. Syntheses, structural characterisation and electronic structures of ferrocenyl-osmafuran heterobinuclear organometallic complexes. *Dalton Trans.* **2017**, *46*, 15803-15811.

[22] (a) Low, P. J. Twists and turns: Studies of the complexes and properties of bimetallic complexes featuring phenylene ethynylene and related bridging ligands. *Coord. Chem. Rev*. **2013**, *257*, 1507-1532; (b) Zhang, J.; Zhang, M.-X.; Sun, C.-F.;

Xu, M.; Hartl, F.; Yin, J.; Yu, G.-A.; Rao, L.; Liu, S.-H. Diruthenium Complexes with Bridging Diethynyl Polyaromatic Ligands: Synthesis, Spectroelectrochemistry, and Theoretical Calculations. *Organometallics* **2015**, *34*, 3967-3978; (c) Zhong, Y.-W.; Gong, Z.-L.; Shao, J.-Y.; Yao, J.-N. Electronic coupling in cyclometalated ruthenium complexes. *Coord. Chem. Rev*. **2016**, *312*, 22-40; (d) Cao, Z.; Xi, B.; Jodoin, D. S.; Zhang, L.; Cummings, S. P.; Gao, Y.; Tyler, S. F.; Fanwick, P. E.; Crutchley, R. J.; Ren, T. Diruthenium–Polyyn-diyl–Diruthenium Wires: Electronic Coupling in the Long Distance Regime. *J. Am. Chem. Soc*. **2014**, *136*, 12174-12183.

[23] (a) Lambert, C.; Nöll, G. The Class II/III Transition in Triarylamine Redox Systems. *J. Am. Chem. Soc*. **1999**, *121*, 8434-8442; (b) Zhou, G.; Baumgarten, M.; Müllen, K. Arylamine-Substituted Oligo(ladder-type pentaphenylene)s: Electronic Communication between Bridged Redox Centers. *J. Am. Chem. Soc*. **2007**, *129*, 12211-12221; (c) Lambert, C.; Nöll, G.; Schelter, J. Bridge-mediated hopping or superexchange electron-transfer processes in bis(triarylamine) systems. *Nat. Mater*. **2002**, *1*, 69-73; (d) Jones, S. C.; Coropceanu, V.; Barlow, S.; Kinnibrugh, T.; Timofeeva, T.; Brédas, J. L.; Marder, S. R. Delocalization in Platinum−Alkynyl Systems: A Metal-Bridged Organic Mixed-Valence Compound. *J. Am. Chem. Soc*. **2004**, *126*, 11782-11783; (e) Barlow, S.; Risko, C.; Chung, S.-J.; Tucker, N. M.; Coropceanu, V.; Jones, S. C.; Levi, Z.; Brédas, J.-L.; Marder, S. R. Intervalence Transitions in the Mixed-Valence Monocations of Bis(triarylamines) Linked with Vinylene and Phenylene−Vinylene Bridges. *J. Am. Chem. Soc*. **2005**, *127*, 16900-16911; (f) Heckmann, A.; Amothor, S.; Lambert, C. Mulliken–Hush analysis of a bis(triarylamine) mixed-valence system with a N···N distance of 28.7 Å. *Chem. Commun*. **2006**, 2959-2961; (g) Lacroix, J. C.; Chane-Ching, K. I.; Maquère, F.; Maurel, F. Intrachain Electron Transfer in Conducting Oligomers and Polymers: The Mixed Valence Approach. *J. Am. Chem. Soc*. **2006**, *128*, 7264-7276; (h) Amthor, S.; Lambert, C. [2.2]Paracyclophane-Bridged Mixed-Valence Compounds:

Application of a Generalized Mulliken−Hush Three-Level Model. *J. Phys. Chem. A* **2006**, *110*, 1177-1189; (i) Sakamoto, R.; Sasaki, T.; Honda, N.; Yamamura, T. 5,15-Bis(di-p-anisylamino)-10,20-diphenylporphyrin: distant and intense electronic communication between two amine sites. *Chem. Commun*. **2009**, 5156-5158; (j) He, B.; Wenger, O. S. Photoswitchable Organic Mixed Valence in Dithienylcyclopentene Systems with Tertiary Amine Redox Centers. *J. Am. Chem. Soc*. **2011**, *133*, 17027-17036; (k) Yao, C.-J.; Zheng, R.-H.; Shi, Q.; Zhong, Y.-W.; Yao. J. 1,4-Benzene-bridged covalent hybrid of triarylamine and cyclometalated ruthenium: a new type of organic–inorganic mixed-valent system. *Chem. Commun*. **2012**, *48*, 5680-5682.

[24] (a) Lambert, C.; Risko, C.; Coropceanu, V.; Schelter, J.; Amthor, S.; Gruhn, N. E.; Durivage, J. C.; Brédas, J.-L. Electronic Coupling in Tetraanisylarylenediamine Mixed-Valence Systems: The Interplay between Bridge Energy and Geometric Factors. *J. Am. Chem. Soc*. **2005**, *127*, 8508-8516; (b) Kattnig, D. R.; Mladenova, B.; Grampp, G.; Kaiser, C.; Heckmann, A.; Lambert, C. Electron Paramagnetic Resonance Spectroscopy of Bis(triarylamine) Paracyclophanes as Model Compounds for the Intermolecular Charge-Transfer in Solid State Materials for Optoelectronic Applications. *J. Phys. Chem. C* **2009**, *113*, 2983-2995.

[25] Ning, Z.; Tian, H. Triarylamine: a promising core unit for efficient photovoltaic materials. *Chem. Commun*. **2009**, 5483-5495.

[26] Zhang, M.-X.; Zhang, J.; Yin, J.; Hartl, F.; Liu, S.-H. Anodic electrochemistry of mono- and dinuclear aminophenylferrocene and diphenylaminoferrocene complexes. *Dalton Trans*. **2018**, *47*, 6112-6123.

[27] Liu, B.; Xie, H.; Wang, H.; Wu, L.; Zhao, Q.; Chen, J.; Wen, T. B.; Cao, Z.; Xia, H. Selective Synthesis of Osmanaphthalene and Osmanaphthalyne by Intramolecular C-H Activation. *Angew. Chem. Int. Ed*. **2009**, *48*, 5461-5464.

[28] Zhang, M.-X.; Xu, Z.; Lu, T.; Yin, J.; Liu, S. H. A Visible-Light-Induced Strategy

to Construct Osmanaphthalynes, Osmaanthracyne and Osmaphenanthryne. *Chem. Eur. J.* **2018**, doi: 10.1002/chem.201803576.

[29] Jia, G. Recent progress in the chemistry of osmium carbyne and metallabenzyne complexes. *Coord. Chem. Rev.* **2007***, 251*, 2167–2187.

[30] Bolaño, T.; Castarlenas, R.; Esteruelas, M. A.; Oñate, E. Hydride-Carbyne to Carbene Transformation in an Osmium-Acetate-Bis(triisopropylphosphine) System: Influence of the Coordination Mode of the Carboxylate and the Reaction Solvent. *Organometallics* **2007**, *26*, 2037-2041.

[31] Bolaño, T.; Castarlenas, R.; Esteruelas, M. A.; Modrego, F. J.; Oñate, E. Hydride-Alkenylcarbyne to Alkenylcarbene Transformation in Bisphosphine-Osmium Complexes. *J. Am. Chem. Soc*. **2005**, *127*, 11184-11195.

[32] (a) Castro-Rodrigo, R.; Esteruelas, M. A.; López, A. M.; Oñate, E. Reactions of a Dihydrogen Complex with Terminal Alkynes: Formation of Osmium−Carbyne and −Carbene Derivatives with the Hydridotris(pyrazolyl)borate Ligand. *Organometallics* **2008**, *27*, 3547-3555; (b) Bolaño, T.; Castarlenas, R.; Esteruelas, M. A.; Oñate, E. Sequential and Selective Hydrogenation of the C_α−C_β and M−C_α Double Bonds of an Allenylidene Ligand Coordinated to Osmium: New Reaction Patterns between an Allenylidene Complex and Alcohols. *J. Am. Chem. Soc*. **2007**, *129*, 8850-8859.

[33] (a) Esteruelas, M. A.; Hernández, Y. A.; López, A. M.; Oliván, M.; Oñate, E. Reduction and C(sp^2)−H Bond Activation of Ketones Promoted by a Cyclopentadienyl-Osmium- Dihydride-Dihydrogen Complex. *Organometallics* **2005**, *24*, 5989-6000; (b) Buil, M. L.; Esteruelas, M. A.; Goni, E.; Oliván, M.; Oñate, E. Displacement of Phenyl and Styryl Ligands by Benzophenone Imine and 2-Vinylpyridine on Ruthenium and Osmium. *Organometallics* **2006**, *25*, 3076-3083; (c) Esteruelas, M. A.; Gutiérrez-Puebla, E.; López, A. M.; Oñate, E.; Tolosa, J. I. Reactions of Os(η^5-C_5H_5)Cl($PiPr_3$)$_2$ with $NHCPh_2$ and PPh_3: The Unit Os(η^5-

C_5H_5)($PiPr_3$) as Support for the Study of the Competitive Alkane−Arene Intramolecular C−H Activation. *Organometallics* **2000**, *19*, 275-284.

[34] He, G.; Zhu, J.; Hung, W. Y.; Wen, T. B.; Sung, H. H.-Y.; Williams, I. D.; Lin, Z.; Jia, G. A Metallanaphthalyne Complex from Zinc Reduction of a Vinylcarbyne Complex. *Angew. Chem. Int. Ed*. **2007**, *46*, 9065-9068.

[35] Kaim, W.; Kohlmann, S.; Ernst, S.; Olbrich-Deussner, B.; Bessenbacher, C.; Schulz, A. What determines the solvatochromism of metal-to-ligand charge transfer transitions? A demonstration involving 17 tungsten carbonyl complexes. *J. Organometal. Chem.* **1987**, *321*, 215-226.

[36] Deng, S.-L.; Chen, T.-L.; Chien, W.-L.; Hong, J.-L. Aggregation-enhanced emission in fluorophores containing pyridine and triphenylamine terminals: restricted molecular rotation and hydrogen-bond interaction. *J. Mater. Chem. C* **2014**, *2*, 651-659.

[37] Jin, H.; Li, X.; Tan, T.; Wang, S.; Xiao, Y.; Tian, J. Electrochromic properties of novel chalcones containing triphenylamine moiety. *Dyes and Pigments* **2014**, *106*, 154-160.

[38] Rizalman, N. S.; Capel Ferrón, C.; Niu, W.; Wallace, A. L.; He, M.; Balster, R.; Lampkin, J.; Hernández, V.; López Navarrete, J. T.; Ruiz Delgado, M. C.; Hartl, F. Radical cations of end-capped tetrathienoacenes and their π-dimerization controlled by the nature of α-substituents and counterion concentration. *RSC Adv.* **2013**, *3*, 25644-25647.

[39] Sheldrick, G. M. SHELXS-97, a Program for Crystal Structure Solution; University of Göttingen: Göttingen, Germany, **1997**.

[40] Sheldrick, G. M. Crystal Structure Refinement with SHELXL. *Acta Cryst*. **2015**, *C71*, 3-8.

[41] Krejčík, M.; Daněk, M.; Hartl, F. Simple construction of an infrared optically transparent thin-layer electrochemical cell: Applications to the redox reactions of

ferrocene, $Mn_2(CO)_{10}$ and $Mn(CO)_3$(3, 5-di-t-butyl-catecholate)$^-$. *J. Electroanal. Chem. Interfacial Electrochem*. **1991**, *317*, 179-187.

[42] Gaussian 09, Revision D.01, Frisch, M. J.; Trucks, G. W.; Schlegel, H. B.; Scuseria, G. E.; Robb, M. A.; Cheeseman, J. R.; Scalmani, G.; Barone, V.; Mennucci, B.; Petersson, G. A.; Nakatsuji, H.; Caricato, M.; Li, X.; Hratchian, H. P.; Izmaylov, A. F.; Bloino, J.; Zheng, G.; Sonnenberg, J. L.; Hada, M.; Ehara, M.; Toyota, K.; Fukuda, R.; Hasegawa, J.; Ishida, M.; Nakajima, T.; Honda, Y.; Kitao, O.; Nakai, H.; Vreven, T.; Montgomery, J. A., Jr.; Peralta, J. E.; Ogliaro, F.; Bearpark, M.; Heyd, J. J.; Brothers, E.; Kudin, K. N.; Staroverov, V. N.; Kobayashi, R.; Normand, J.; Raghavachari, K.; Rendell, A.; Burant, J. C.; Iyengar, S. S.; Tomasi, J.; Cossi, M.; Rega, N.; Millam, J. M.; Klene, M.; Knox, J. E.; Cross, J. B.; Bakken, V.; Adamo, C.; Jaramillo, J.; Gomperts, R.; Stratmann, R. E.; Yazyev, O.; Austin, A. J.; Cammi, R.; Pomelli, C.; Ochterski, J. W.; Martin, R. L.; Morokuma, K.; Zakrzewski, V. G.; Voth, G. A.; Salvador, P.; Dannenberg, J. J.; Dapprich, S.; Daniels, A. D.; Farkas, Ö.; Foresman, J. B.; Ortiz, J. V.; Cioslowski, J.; Fox, D. J. Gaussian, Inc., Wallingford CT, **2009**.

[43] (a) Becke, A. D. Density-functional thermochemistry. III. The role of exact exchange. *J. Chem. Phys.* **1993**, *98*, 5648–5652; (b) Lee, C.; Yang, W.; Parr, R. G. Development of the Colle-Salvetti correlation-energy formula into a functional of the electron density. *Phys. Rev. B* **1988**, *37*, 785-789.

[44] (a) Barone, V.; Cossi, M. Quantum Calculation of Molecular Energies and Energy Gradients in Solution by a Conductor Solvent Model. *J. Phys. Chem. A* **1998**, *102*, 1995-2001; (b) Cossi, M.; Rega, N.; Scalmani, G.; Barone, V. Energies, structures, and electronic properties of molecules in solution with the C-PCM solvation model. *J. Comput. Chem*. **2003**, *24*, 669-681.

TOC and Graphical Abstract

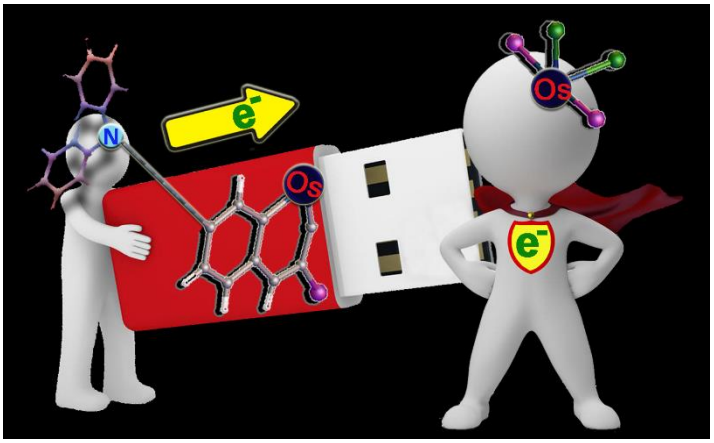

Two intriguing diphenylamino (DPA)-substituted heterocyclic osmanaphthalyne complexes were successfully synthesized and characterized. They show remarkable non-solvatochromic charge transfer absorption in the visible region, proving electronic communication between the donor DPA and acceptor metallacycle redox centers. Results of combined spectro-electrochemical and DFT studies reveal that the spin density in the singly oxidized osmanaphtalynes is dominantly residing on the aminyl segment. In the reference unsubstituted osmanaphthalyne, both one-electron oxidation and reduction are localized on the metallacycle.

Ming-Xing Zhang, Jing Zhang, Xuyang Jin, Xiaona Sun, Jun Yin, František Hartl,, Sheng Hua Liu**

Page No. – Page No.

Title: Diphenylamine-Substituted Osmanaphthalyne Complexes: Structural, Bonding and Redox Properties of Unusual Donor−Bridge−Acceptor Systems